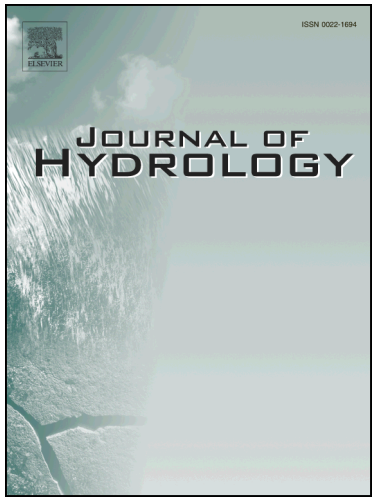
Accepted Manuscript



Research papers

Spatiotemporal patterns of precipitation inferred from streamflow observations across the Sierra Nevada mountain range

Brian Henn, Martyn P. Clark, Dmitri Kavetski, Andrew J. Newman, Mimi Hughes, Bruce McGurk, Jessica D. Lundquist

PII: S0022-1694(16)30488-7
DOI: http://dx.doi.org/10.1016/j.jhydrol.2016.08.009
Reference: HYDROL 21444

To appear in: *Journal of Hydrology*

Received Date: 1 April 2016
Revised Date: 14 July 2016
Accepted Date: 7 August 2016

Please cite this article as: Henn, B., Clark, M.P., Kavetski, D., Newman, A.J., Hughes, M., McGurk, B., Lundquist, J.D., Spatiotemporal patterns of precipitation inferred from streamflow observations across the Sierra Nevada mountain range, *Journal of Hydrology* (2016), doi: http://dx.doi.org/10.1016/j.jhydrol.2016.08.009

This is a PDF file of an unedited manuscript that has been accepted for publication. As a service to our customers we are providing this early version of the manuscript. The manuscript will undergo copyediting, typesetting, and review of the resulting proof before it is published in its final form. Please note that during the production process errors may be discovered which could affect the content, and all legal disclaimers that apply to the journal pertain.

ACCEPTED MANUSCRIPT

Spatiotemporal patterns of precipitation inferred from streamflow observations across the Sierra Nevada mountain range

Brian Henn[a,*], Martyn P. Clark[b], Dmitri Kavetski[c], Andrew J. Newman[d], Mimi Hughes[e], Bruce McGurk[f] and Jessica D. Lundquist[g]

[a] Department of Civil and Environmental Engineering, University of Washington, 201 More Hall, Box 352700, Seattle, WA 98195, USA; bhenn@u.washington.edu

[b] Research Applications Laboratory, National Center for Atmospheric Research, Boulder, CO, USA; mclark@ucar.edu

[c] School of Civil, Environmental and Mining Engineering, University of Adelaide, Adelaide, South Australia, Australia; dmitri.kavetski@adelaide.edu.au

[d] Research Applications Laboratory, National Center for Atmospheric Research, Boulder, CO, USA; anewman@ucar.edu

[e] National Oceanic and Atmospheric Administration, Earth System Research Laboratory, Physical Sciences Division, Boulder, CO, USA; mimi.hughes@noaa.gov

[f] McGurk Hydrologic, Orinda, CA, USA; brucemcgurk@comcast.net

[g] Department of Civil and Environmental Engineering, University of Washington, Seattle, WA, USA; jdlund@u.washington.edu

* Corresponding Author

For submission to the Journal of Hydrology special issue on precipitation (March 2016)

ACCEPTED MANUSCRIPT

Abstract: Given uncertainty in precipitation gauge-based gridded datasets over complex terrain, we use multiple streamflow observations as an additional source of information about precipitation, in order to identify spatial and temporal differences between a gridded precipitation dataset and precipitation inferred from streamflow. In particular, we test whether gridded datasets capture across-crest and regional spatial patterns of variability, as well as year-to-year variability and trends in precipitation, in comparison to precipitation inferred from streamflow. We use a Bayesian model calibration routine with multiple lumped hydrologic model structures to infer the most likely basin-mean, water-year total precipitation for 56 basins with long-term (>30 year) streamflow records in the Sierra Nevada mountain range of California. We compare basin-mean precipitation derived from this approach with basin-mean precipitation from a precipitation gauge-based, 1/16° gridded dataset that has been used to simulate and evaluate trends in Western United States streamflow and snowpack over the 20th century. The long-term average spatial patterns differ: in particular, there is less precipitation in the gridded dataset in higher-elevation basins whose aspect faces prevailing cool-season winds, as compared to precipitation inferred from streamflow. In some years and basins, there is less gridded precipitation than there is observed streamflow. Lower-elevation, southern, and east-of-crest basins show better agreement between gridded and inferred precipitation. Implied actual evapotranspiration (calculated as precipitation minus. streamflow) then also varies between the streamflow-based estimates and the gridded dataset. Absolute uncertainty in precipitation inferred from streamflow is substantial, but the signal of basin-to-basin and year-to-year differences are likely robust. The findings suggest that considering streamflow when spatially distributing precipitation in complex terrain may improve the representation of basins whose orientations (e.g., windward-facing) are favored for orographic precipitation enhancement.

Highlights:

- We use unimpaired observations from 56 long-term stream gauges in the Sierra Nevada
- We infer precipitation from streamflow for each basin-year with lumped hydrologic models
- For each year precipitation inferred from streamflow compared to gridded estimates
- Gridded estimates underestimate precipitation in basins favored for upslope flow
- Precipitation inferred from streamflow reveals inter-annual spatial variability

Keywords: Precipitation; orographic enhancement; streamflow; mountain hydrology; Sierra Nevada; Bayesian inference

ACCEPTED MANUSCRIPT

1. Introduction

1.1. Approach for reducing uncertainty in distributed precipitation estimates in complex terrain

Mountainous areas in the mid-latitudes develop snowpack that is critical for water resources and ecosystems services; thus, they serve as "water towers" for the world (Viviroli et al., 2007). Over complex terrain in the mid-latitudes, precipitation observations are generally limited to in situ gauge observations, due to challenges in remote sensing of mountain precipitation with ground-based radar (Westrick et al., 1999) and satellite-based methods (Lettenmaier et al., 2015). As a result, it has been necessary to develop methods to distribute or interpolate gauge-based observations across the landscape to a grid (e.g., Daly et al., 2008; Newman et al., 2015; Thornton et al., 1997), while attempting to account for the strong topographic influences on spatiotemporal patterns of precipitation (Roe, 2005).

Large uncertainties can occur during estimation of spatially distributed precipitation (e.g., Gutmann et al., 2012; Henn et al., 2016, this issue; Livneh et al., 2014), due to both sparse and uncertain gauge data in mountainous areas (Lundquist et al., 2003; Rasmussen et al., 2011a; Sieck et al., 2007) and uncertainty in the interpolation of gauge data to a grid (Clark and Slater, 2006). As a result, it may be useful to apply other types of observations and estimates to infer precipitation in these areas and reduce potential errors in gridded datasets. Streamflow observations offer an additional method with which to infer precipitation patterns and evaluate gridded precipitation datasets. Streamflow has been used to correct gridded precipitation products for high-elevation underestimation at the global scale (Adam et al., 2006), to evaluate sources of precipitation data (Wayand et al., 2013) and precipitation distribution schemes (Le Moine et al., 2015; Livneh et al., 2014) at the basin scale, and to identify errors in precipitation forcing data in hydrologic models (McMillan et al., 2011b; Renard et al., 2010). In general, these

ACCEPTED MANUSCRIPT

studies have shown that substantial errors in spatially distributed precipitation can be identified through a comparison with observed streamflow.

Henn et al. (2015) developed an approach for inferring basin-mean precipitation from streamflow in the Yosemite National Park region of the Sierra Nevada mountain range of California, and tested the sensitivity of the inferred precipitation from this approach to various assumptions. Their approach uses Bayesian calibration of simple snow and hydrologic models to estimate the most likely water-year total precipitation in a basin given daily streamflow observations. In effect, this approach calibrates the models to match streamflow under uncertain precipitation inputs; the models estimating the actual evapotranspiration (ET) needed to close the basin's water balance. They used a small ensemble of six hydrologic model structures to estimate the uncertainty of the inferred precipitation associated with model structural assumptions. Based on seven Yosemite-area basins tested in Henn et al. (2015), they concluded that streamflow allows for robustly inferring the climatological patterns of precipitation across the mountain range, i.e., identifying wetter and dryer areas within the range. Streamflow also highlighted annual variability between wet and dry years. They also found that long-term inferred basin-mean precipitation disagreed by up to 25% with Parameter Regression on Independent Slopes Model (PRISM; Daly et al., 2008, 2002, 1994) precipitation climatology. However, the absolute amounts of inferred precipitation are sensitive to the model structures used to simulate the basins, suggesting that this approach is only suited for identifying errors greater than 100 mm yr^{-1} in spatially distributed precipitation estimates.

1.2. Study objectives and contents

This paper further develops the approach of Henn et al. (2015) and extends it to a spatial domain encompassing a large mountain range. We describe a streamflow dataset from the Sierra

ACCEPTED MANUSCRIPT

Nevada, the method for inferring precipitation from streamflow, and a set of experiments to compare inferred precipitation against the gridded precipitation dataset. We apply the approach of inferring precipitation from streamflow in 56 basins in the Sierra Nevada that have largely unimpaired, long-term streamflow observations. We do this to compare inferred precipitation against the Hamlet et al. (2010) 1/16° gridded daily precipitation dataset (hereafter H10) over water years 1950-2010. We choose this dataset as it has been used to resolve spatial patterns and trends in Western United States snowpack and streamflow (Hamlet et al., 2007, 2005), and because it explicitly attempts to reduce temporal inhomogeneity by using long-term station records to control trends in the precipitation data (Hamlet and Lettenmaier, 2005). It also utilizes PRISM precipitation climatology as its long-term mean spatial pattern in order to account for topographic effects.

We do this to identify patterns of where and when precipitation estimates diverge in the Sierra Nevada. Based on examinations of differences between gridded precipitation datasets (Henn et al., 2016b, this issue), we hypothesize that areas of high elevation and complex terrain where precipitation gauge density is low may have substantial biases in gridded precipitation datasets, and these biases can be identified by precipitation inferred from streamflow. Research on orographic precipitation has shown that properly-oriented topography can induce steep spatial gradients in precipitation rates (Roe, 2005); we hypothesize that these biases may be greatest in areas that are favorable for orographic precipitation enhancement, where interpolation may tend to perform poorly. We use precipitation inferred from streamflow to evaluate whether gridded precipitation datasets capture areas of orographic enhancement, the ratios of windward to leeward precipitation (i.e., rain shadows), year-to-year variability in the spatial patterns of precipitation, and long-term trends in basin-mean precipitation.

ACCEPTED MANUSCRIPT

We are unaware of previous studies that have used many distributed streamflow observations to infer orographic precipitation patterns over a mountain range over long timescales. We use a large number (56) of stream gauges distributed over a ~400km long mountain range, both on the windward and leeward slopes, and we use streamflow observations that span multiple decades at each gauge. Thus, we are able to consider both annual spatial patterns of streamflow and precipitation, as well as year-to-year variability and long-term trends in those patterns.

Unlike Henn et al. (2015), here we develop quantitative estimates of prior uncertainty in basin-mean precipitation for Bayesian inference by considering the agreement (or lack thereof) between independent precipitation data sources for each basin. For example, numerical weather prediction of precipitation over complex terrain has improved in fidelity as models have been run at higher resolution and with more process-based microphysical parameterizations (e.g., Rasmussen et al., 2011b). The Weather Research and Forecasting model (WRF, Skamarock and Klemp, 2008) has been shown to generate precipitation estimates that are equal or better in terms of simulated hydrologic responses, as compared to gauge-based gridded precipitation, in some mountain basins (Gutmann et al., 2012; Wayand et al., 2013). Thus, we consider WRF precipitation as a source of information about the patterns of precipitation over complex terrain. We also consider a gridded precipitation dataset (Newman et al., 2015) that does not depend on PRISM climatology, along with the H10 dataset, as part of our prior estimate of basin-mean precipitation.

Sections 2 and 3 describe the data and models, respectively, used in the inference of precipitation from streamflow. Section 4 presents the results of the precipitation inference and the comparison against the gridded dataset. Section 5 discusses the implications of the

ACCEPTED MANUSCRIPT

differences between gridded and inferred precipitation, and the potential value of streamflow observations for gridded precipitation datasets. Section 6 offers conclusions from the study.

2. Data

In this section we describe the data used to compare H10 gridded precipitation with precipitation inferred from streamflow: unimpaired daily streamflow observations, basin topography and soils information, gridded precipitation data from several sources, and gridded temperature and evapotranspiration data.

2.1. Streamflow and basins

For comparison against precipitation, we identify 56 basins in the Sierra Nevada (Figure 1; Table 1) in which daily streamflow observations have been made for extended periods of time. Forty-one of the gauges are west of the crest of the Sierra Nevada, and 15 are on the east slope. Streamflow observations included in this study have at least 30 water years of complete or nearly complete records between 1950 and 2010; in a few cases we include stream gauges with 20-30 years of data because they were in areas with few gauges (the southeastern Sierra Nevada). Thirty-one of the 56 continue to operate, and 34 are listed in the Hydro-Climate Data Network (HCDN) of basins without significant regulation from dams or diversions to agricultural or domestic use (Slack and Landwehr, 1992). We also include 22 basins not in the HCDN but with relatively few or "small" impairments, based on descriptions provided by the United States Geological Survey (USGS) water data reports for each site (Anderson et al., 1996; Rockwell et al., 1996a, 1996b). In a few cases, we include basins with upstream dam regulation, so long as the storage was small compared to annual runoff volumes, or the regulation effect could be removed from the streamflow record because complete storage records were available. We

ACCEPTED MANUSCRIPT

exclude most stream gauges with observations that were described as having poor quality by the USGS; 3 gauges in the southeastern Sierra Nevada rated "poor" (Big Pine Cr., Independence Cr. and Cottonwood Cr.) were included due to a lack of gauges in this area. All streamflow data were downloaded from the USGS National Water Information System Web Interface (http://waterdata.usgs.gov/nwis/sw), with the exception of two basins (Cherry-Eleanor and the Tuolumne River at Hetch Hetchy), in which full natural flows were provided by the operator of the reservoirs at the basin outlets, Hetch Hetchy Water and Power; see supplemental material of Henn et al. (2015). More detailed information on the individual stream gauges and their associated basins is included in Table 1.

The USGS streamflow measurements are made by translating direct stream stage measurements into discharge via streamflow rating curves. Rating curves are developed and updated using direct measurements of discharge, but they are subject uncertainty. Discharge uncertainty due to rating curve errors have been estimated at 10% for observations of "good" quality, and 15% for "fair" records (Rockwell et al., 1996a), in that 95% of the daily measurements should fall within the stated margin of error. While other studies of other rating curve-based streamflow techniques have suggested uncertainties of up to 20-40% at very high flows (Baldassarre and Montanari, 2009), we are primarily interested in precipitation and runoff over timescales of a water year or longer, and so we presume the USGS estimates to be a reasonable representation of uncertainty.

Topographical boundaries of the basins are delineated based on 30 m USGS elevation data, which are also used to calculate basin area distributions within 100 m elevation bands. The basins' areas (Table 1) range from 10.1 km^2 (Daggett Cr.) to 3,472 km^2 (Kings R.); the median

ACCEPTED MANUSCRIPT

basin area is 165 km^2. The basins' mean elevations range from 744 m (White R.) to 3,457 m (Middle Fork of Bishop Cr.); most basins span at least 1,500 m in elevation.

We use typical basin soil properties to provide information for the lumped hydrologic model in the inference of precipitation from streamflow (section 3). Most of the basins are near the crest of the Sierra Nevada and have steep topography that is underlain by granitic bedrock. Typical soils in glaciated areas near the crest are shallow and sandy, with a depth of no more than 1 m and a porosity of about 0.4 (NRCS, 2007), though water is likely available for evapotranspiration from deeper in the soil-bedrock interface (Goulden et al., 2012; Rose et al., 2003). Field studies have indicated that soils in higher elevation areas of the Sierra Nevada have high porosities (0.3 to 0.55) and conductivities (1 cm to 1 m d^{-1}) typical of sand and gravel, but that values decline with depth approaching the underlying bedrock, and that soils are deeper and more heterogeneous in lower-elevation areas further from the crest (Bales et al., 2011; Flint et al., 2008; Holbrook et al., 2014). Calibration ranges for the hydrologic model soil parameters (Section 3) reflect these values.

2.2. Gridded precipitation

To force the hydrologic models, time series of precipitation, temperature and potential evapotranspiration (PET) are needed for each basin. Here we describe the gridded precipitation datasets that provide the precipitation forcing data; temperature and PET data sources are described in Section 2.3.

2.2.1. H10 precipitation

We use the H10 daily precipitation dataset as a basis for comparison with streamflow and precipitation inferred from streamflow. The dataset uses National Weather Service Cooperative Observer (NWS COOP) daily precipitation gauge observations, and the PRISM 1971-2000

ACCEPTED MANUSCRIPT

monthly precipitation climatology (Daly et al., 2008, 2002, 1994) as a topographic corrector in the interpolation of gauge precipitation over complex terrain. We choose this dataset because of its relatively high spatial resolution (1/16°, ~6 km) and long-term span (1915-2010 over California), and because H10 and its predecessors have been used to simulate snow and streamflow in Western United States (e.g., Mote et al., 2005). However, we note that other long-term gridded datasets (Livneh et al., 2015; PRISM Climate Group, 2015) are also available.

Here we use H10 data covering water years 1950-2010 (water year 1949 is used for model spin-up), over a spatial domain which covers the streamflow basins: from -121.5°W to -117.5°W and from 35.5°N to 40°N. For each basin we calculate the fraction of each H10 grid cell that is within the basin, and calculate the H10 basin-mean time series as the weighted sum of the grid cells' precipitation. We use this daily time series of precipitation, combined with a multiplicative precipitation scaling factor inferred in calibration, to force the hydrologic and snow models that are the basis for inferring precipitation from streamflow for each basin (see section 3).

2.2.2. N15, WRF and other precipitation datasets

In order to estimate the uncertainty of the H10 precipitation estimates and how the uncertainty varies across the Sierra Nevada, we also examine independently-generated gridded precipitation data. A quantitative estimate of precipitation, and its associated uncertainty, is necessary for the Bayesian inference of precipitation from streamflow (see section 3). For one additional source of precipitation information, we use the N15 dataset (Newman et al., 2015); while it interpolates gauge data in a qualitatively similar manner to H10, it does not use PRISM precipitation climatology as a topographic corrector, and thus may be a more independent estimate from H10 than other PRISM-based datasets. N15 is a 100-member ensemble dataset,

ACCEPTED MANUSCRIPT

such that uncertainty in the data can be explicitly quantified. N15 uses a 1/8° (~12 km) spatial grid, and so there may be greater topographic smoothing compared to the 1/16° datasets.

Second, we use WRF model (Skamarock and Klemp, 2008) daily precipitation totals over California. The regional WRF simulations were generated using WRF version 3.6.0 (Skamarock et al., 2008) to dynamically downscale the North American Regional Reanalysis (NARR), with a methodology very similar to that used in Hughes et al. (2012). The WRF downscaling has two nested domains, with an outer 18 km grid extending across the northeastern Pacific and much of the U.S. intermountain west, and a 6 km grid domain that covers all of California, similar to Figure 1 of Hughes et al. (2012). Both domains have 82 vertical levels, with 50-75 m vertical resolution within the lowest 2 km of atmosphere, with model top at 100 hPa. Both domains use Morrison double-moment microphysics (Morrison et al., 2009), Dudhia shortwave radiation (Dudhia, 1989) and RRTM longwave radiation (Mlawer et al., 1997) called every 6 minutes, Kain-Fritsch convective parameterization (Kain, 2004), the Yonsei University planetary boundary layer scheme (Hong et al., 2006), and the Noah land surface model (Tewari et al., 2004). WRF data were generated for 11 calendar years, 2004-2014, and over this time period, the model was re-initialized approximately every 5 days using NARR data, with the first three hours of each 5-day period discarded as model spin-up. The model is run with a 30-second (10-second) time step in the 18 km (6 km) domain; for precipitation, output data are aggregated to daily totals. For both the N15 and WRF precipitation, gridded precipitation is aggregated to single time series for each basin using the fractional grid cells approach described above for H10.

For comparison, we also briefly examine two other gridded precipitation datasets: (Livneh et al., 2015), hereafter L15, and North American Land Data Assimilation System, phase 2 (Cosgrove et al., 2003; Mitchell et al., 2004; Xia et al., 2012), hereafter NLDAS-2. We include

ACCEPTED MANUSCRIPT

these datasets to see whether patterns of differences between gridded and inferred precipitation are consistent across different gridding methodologies. While each gauge-based gridded dataset considered here varies in the set of precipitation gauges used, all of them (with the exception of N15) use PRISM climatology as a topographic corrector. Thus, we hypothesize that spatial patterns of inferred precipitation may be fairly consistent across the gauge-based datasets.

2.3. Temperature and potential evapotranspiration

In addition to precipitation, time series of daily mean temperature and PET are needed to force the hydrologic models that are run for each basin. For temperature, we calculate basin-mean time series of daily high and low temperature from the H10 data in the same fashion as for precipitation, and average the high and low temperatures to create a daily mean temperature series.

PET is estimated using the Makkink equation, which uses temperature and shortwave radiation as predictors (e.g., Cristea et al., 2013). The Bristow-Campbell parameterization is used to estimate shortwave radiation from temperature (Bristow and Campbell, 1984). We calibrate the Bristow-Campbell and Makkink methods using data from the Dana Meadows meteorological station (2,987 m above sea level in Yosemite National Park) for water years 2003 through 2009. Shortwave radiation and temperature are used to calibrate the Bristow-Campbell coefficients A (0.7) and C (2.49). Shortwave radiation, wind speed, temperature and relative humidity are applied to estimate PET using the Penman-Monteith equation, following the methods of Allen et al. (1998); this PET estimate is then used to calibrate the Makkink coefficient (0.668).

H10 daily high and low temperatures for each grid cell are used with the approach above to estimate daily PET at each grid cell in the spatial domain. The grid cells' PET are then aggregated to basin-mean PET series for each basin. Due to reduced diurnal temperature range at

ACCEPTED MANUSCRIPT

higher elevations in the H10 data, PET calculated in this way decreases somewhat with elevation, such that 1,000 m elevation has roughly 20% more PET than 3,000 m elevation (about 1,200 mm yr^{-1} vs 1,000 mm yr^{-1}), though there is substantial grid cell variation for a given elevation. Henn et al. (2015) found that inferred precipitation and inferred actual evapotranspiration are only mildly sensitive to PET, presumably due to the largely water-limited climate of the Sierra Nevada, so we do not investigate the effects of PET further here.

3. Methods

To infer basin-mean, water-year total precipitation from daily streamflow observations, the following steps are applied. H10-based precipitation, temperature and PET forcing data are used to drive snow and hydrologic models for each basin and produce simulated streamflow time series. We simulate all water years from 1950-2010 for which streamflow observations are available for each basin; at least one water year before the start of the analysis (*i.e.*, 1949 for basins with streamflow in 1950) is used for model spin-up and is discarded. The parameters of the models include a multiplicative error correction (Kavetski et al., 2003) on the precipitation time series, along with snow and soil parameters. The simulated runoff is compared to the observed streamflow record, and based on the goodness of fit of the streamflow and the prior likelihood of the model parameters, the Bayesian joint posterior distribution of the parameters is generated. From the posterior distribution of the precipitation multiplier, the corrected basin-mean precipitation can then be calculated. This section describes the snow and hydrologic models and the calibration routine used to infer precipitation from streamflow; for a more detailed description of this approach, see Henn et al. (2015), their Figure 1 and their section 3.

ACCEPTED MANUSCRIPT

3.1. Models

3.1.1. FUSE conceptual hydrologic model structures

We use the Framework for Understanding Structural Errors (FUSE; Clark et al., 2008) to provide a set of conceptual hydrologic models and to evaluate the effects of model structural uncertainty on inferred precipitation (Clark et al., 2011; McMillan et al., 2011a). FUSE provides multiple options for representing soil moisture storage and fluxes, such as ET, surface runoff and baseflow, using a spatially lumped approach with upper and lower soil zones. Streamflow, soil moisture and ET time series are simulated at a daily time step. In this study, multiple FUSE structures are included to estimate the uncertainty of the precipitation inferred from streamflow. We use six model structures previously used to investigate the impact of structure on model performance in the Mahurangi basin in New Zealand (Clark et al., 2011; McMillan et al., 2011a) and to infer precipitation from streamflow and snow observations (Henn et al., 2016a, 2015). For greater details on the FUSE model structures, see Henn et al. (2015) and Clark et al. (2008).

3.1.2. Snow model

Each FUSE structure is coupled to a temperature index snow model based on Snow-17 (Anderson, 2006), which tracks SWE based on precipitation and melt. Precipitation is added to SWE if the air temperature is below a threshold; otherwise, it is treated as rain. Snowmelt is initiated if the air temperature is above a threshold, and is proportional to the temperature above that point:

$$SM = \max\left(\min[f\{T - T_0\}, SWE], 0\right) \quad (1)$$

where SM is snowmelt per time step, f is the snowmelt factor, T is the air temperature, and T_0 is the melt threshold temperature. The melt factor f varies in a sinusoidal manner over the year, with minimum and maximum values on the winter and summer solstices, respectively. The rain-

ACCEPTED MANUSCRIPT

snow partition temperature, melt initiation temperature, and winter and summer melt factors are all inferred parameters. Snowmelt is combined with rainfall, and the two are routed to the soil model, which otherwise simulates fluxes and storages independently of the snow model.

H10 basin-mean precipitation is corrected for errors using a precipitation multiplier M_i, where the subscript i indicates the daily time step:

$$P_i = M_i P_{f,i} \quad (2).$$

Here, $P_{f,i}$ is the H10 basin-mean precipitation, M_i is the multiplier and P_i is the model forcing precipitation, all at time i. The multipliers are defined such that they are different for each water year, but constant within the water year, and each yearly multiplier is inferred in calibration. In this way, we infer water year precipitation from streamflow.

In order to simulate the strong elevation dependence of snow in the Sierra Nevada, the snow model is run at 100 m elevation bands for each basin (unlike the soil model, which is lumped over the entire catchment). For each band, forcing temperature is lapsed to the ith band midpoint elevation:

$$T_i = T_f + \Gamma(z_i - z_f) \quad (3)$$

where T_i is the ith band temperature, T_f is the forcing temperature, z_i is the band midpoint elevation, z_f is the basin's mean elevation (because basin-mean temperature and precipitation forcing is used), and Γ is the temporally-invariant temperature lapse rate (<0, °C km^{-1}), which is also inferred in calibration.

Finally, water fluxes to the lumped soil model are calculated by a weighted average of rain plus snowmelt from each elevation band:

$$F_{soil} = \sum_{i=1}^{n_{bands}} AF_i(R_i + SM_i) \quad (4)$$

ACCEPTED MANUSCRIPT

where F_{soil} is the flux of water to the soil model, and AF_i is the fraction of the basin area, R_i is the rain, and SM_i is the snowmelt, all from band i.

Unlike in Henn et al. (2015) and Henn et al. (2016a), we do not use an orographic precipitation gradient (OPG) to distribute precipitation to the basins' elevation bands and infer intra-basin precipitation distributions. Instead, the multiplier-corrected precipitation is distributed evenly to each elevation band. This is done because the results of those studies indicated that the inference was likely not able to discern intra-basin precipitation patterns; almost all inferred OPGs were at or near zero. Thus, precipitation inferred from streamflow represents the basin-mean amount for each water year. The actual precipitation distribution is, of course, spatially variable within each basin, and distributing the mean precipitation values from this study would be more complex in basins with greater topographic relief.

We choose to use a temperature index snow model instead of a full energy balance snow model. We calibrate the precipitation forcing data, which has large effects on the snow simulation (*e.g.*, Raleigh et al., 2015). The precipitation uncertainty likely overwhelms any improvement in snow simulation that might be gained from using an energy balance model. Additionally, temperature index models have fewer tunable parameters than energy balance models; the additional parameters of an energy balance model would increase the computational burden and parametric uncertainty in the Bayesian inference described below.

3.2. Bayesian model calibration

3.2.1. Bayesian inference of precipitation

We infer basin-mean precipitation from streamflow using Bayes' Theorem with the Bayesian Total Error Analysis package (BATEA; Kavetski et al., 2006a). The joint posterior probability density function (PDFs) of the multipliers M and other model parameters θ (the snow

ACCEPTED MANUSCRIPT

and soil parameters and the lapse rate), given observed precipitation $\tilde{P}$ and streamflow $\tilde{Q}$, are described by:

$$\boldsymbol{P}\left(M,\theta\middle|\tilde{Q},\tilde{P}\right)\propto\boldsymbol{P}\left(\tilde{Q}\middle|\mathrm{M},\theta,\tilde{P}\right)\cdot\boldsymbol{P}(M,\theta) \qquad (5).$$

The first product term on the right hand side of (5) is the likelihood function, which describes the probability distribution of the observed streamflow, given particular values of M, θ and the observed gauge precipitation $\tilde{P}$. The likelihood function interprets the difference between observed and simulated streamflow, using an error model. The second product term in (5) is composed of the prior distributions of the precipitation multiplier and other model parameters. The posterior distribution of the precipitation multiplier and the model parameters, $\boldsymbol{P}\left(M,\theta\middle|\tilde{Q},\tilde{P}\right)$, is an update of the prior distributions given streamflow and precipitation observations.

We use a weighted least squares (WLS) residual error model to translate differences between modeled and observed streamflow into the likelihood of the corresponding parameter sets. In the WLS approach, it is assumed that higher streamflow is subject to greater uncertainty, unlike simple least squares in which all time steps are treated equally. Following Thyer et al. (2009), we assume that residual streamflow errors follow a Gaussian distribution with zero mean and a standard deviation that is a linear function of streamflow, *i.e.*,

$$\sigma_t = a\hat{Q}_t + b \qquad (6)$$

where a and b are residual error parameters inferred in the calibration, and $\hat{Q}_t$ is the modeled streamflow at a given time step, t. The error model calculates likelihood as a function of the squared differences between observed and modeled streamflow, which are first normalized at each time step by σ_t.

ACCEPTED MANUSCRIPT

The combination of the soil, snow and yearly multiplier parameters results in a parameter space with 50-80 dimensions, and so to sample the posterior probability distributions, multiple-start Quasi-Newton optimization and a Monte Carlo Markov Chain (MCMC) routine are used within BATEA (Kavetski et al., 2006b). The result of the MCMC sampling routine is an ensemble of parameter sets, with more samples clustered around parameter values of greater posterior probability.

Henn et al. (2016a) considered the use of snow observations in addition to streamflow to infer precipitation, which yielded a reduction in the uncertainty of inferred precipitation and also showed sensitivity to the estimate of basin-mean SWE. Because we lack robust methods for estimating basin-mean SWE across Sierra Nevada basins (generally, only point measurements of SWE are available), we use only streamflow to infer precipitation.

3.2.2. Parameter prior distributions

To constrain the inference within the Bayesian framework, prior distributions are placed on the multiplier and each hydrologic and snow model parameter. We use similar snow and soil parameter distributions as in Henn et al. (2015): uniform distributions are generally used, and when no information is available about a parameter in the study domain, the distribution is set to the default limits for the FUSE model (Clark et al., 2008). For more details on the soil and snow model parameters, see Table 1 of Henn et al. (2015).

The prior distributions of the precipitation multipliers are normal distributions and each yearly multiplier is independent of the others. We use estimates of each basin's mean precipitation, and the differences in precipitation estimates between H10, N15 and WRF, to set the mean and standard deviation of the multipliers' prior distribution.

For the mean of the prior distribution we use:

ACCEPTED MANUSCRIPT

$$\mu_M = \left(P_{H10} + \overline{P}_{N15} + P_{WRF}\right)/(3P_{H10}) \quad (7)$$

where P_{H10}, $\overline{P}_{N15}$ and P_{WRF} are the H10, N15 and WRF basin-mean precipitation for the water year; N15 precipitation is the mean of the ensembles. For each basin, (7) is applied over each water year from 2005 to 2010, and then averaged. In other words, the mean of the prior distribution for each basin is the average of the three datasets' precipitation, divided by the H10 precipitation; this is an *a priori* guess of how H10 precipitation should be corrected, before considering streamflow (see H10, N15 and WRF precipitation in Figures 2a and 2b).

For the standard deviation of the distribution we use:

$$\sigma_M = \frac{1}{\overline{P}}\sqrt{\frac{1}{3}\left(\left[P_{H10} - \overline{P}\right]^2 + \left[P_{N15} - \overline{P}\right]^2 + \left[P_{WRF} - \overline{P}\right]^2\right)} \quad (8)$$

where $\overline{P}$ is the mean precipitation of the three datasets, or:

$$\overline{P} = \mu_M P_{H10} \quad (9).$$

Thus, the standard deviation of the multiplier prior distribution is the standard deviation of basin precipitation in H10, N15 and WRF, normalized by the mean of the three. As with the mean, (8) is applied to estimate the standard deviation for each year from 2005 to 2010 and then averaged; this process is repeated for each of the basins. Thus, we use the agreement between the three datasets (or lack thereof) to estimate the prior distribution of uncertainty in precipitation for a given basin. All multipliers are drawn from the same prior distribution, but each year's multiplier is unique and independent of the other years' multipliers.

To illustrate this process for the Cherry-Eleanor basin, the three datasets' precipitation time series are shown in Figure 2a and are mapped for water year 2008 in Figures 2b-d, and the resulting prior distribution is plotted for water year 2008 in Figure 2e. We first plot the different precipitation estimates over time for this basin, showing the 2005-2010 comparison on which the

ACCEPTED MANUSCRIPT

multipliers' prior distribution is based. The H10 precipitation is generally less than N15 and WRF, and so the mean prior estimate of the multiplier is 1.48 for this basin. The disagreement between the different datasets is also relatively high compared to other basins, with the three sources of precipitation spanning 600-800 mm yr^{-1}. Therefore, the relative standard deviation of the prior distribution is set to reflect this at 0.26; together with the mean, this indicates that prior to considering streamflow, we expect basin-mean precipitation to be between 0.97 and 1.99 times H10 precipitation with 95% confidence. Using water year 2008 (boxed, Figure 2a, and mapped, Figures 2b-2d) as an example, the prior distribution is plotted as a precipitation distribution for Cherry-Eleanor in Figure 2e, i.e., as the product of the multiplier distribution and the 840 mm of precipitation from H10. We also plot water year 2008 streamflow (790 mm) and N15 (1,052 mm) and WRF precipitation (1,499 mm), showing that the prior distribution largely spans the three precipitation data sources.

4. Results

4.1. Experimental approach

First, we examine the Bayesian inference of precipitation, comparing the prior distribution of the multiplier with the posterior distribution for each of the six FUSE model structures. This comparison allows us to evaluate whether the choice of prior distribution and precipitation uncertainty appears appropriate given the precipitation inferred from streamflow, as well as the uncertainty in inferred precipitation associated with the choice of model structure.

Next, we compare H10 precipitation and precipitation inferred from streamflow across the 56 study basins in the Sierra Nevada, at several timescales. We present results for several water years, focusing on those for which many streamflow gauges were operational (1983 and

ACCEPTED MANUSCRIPT

1977), which allows for greater spatial comparison of precipitation. We also compare inferred precipitation and streamflow to other gridded precipitation datasets (to test whether the findings are consistent across different methodologies). Then we present long-term average differences between gridded and inferred precipitation. When testing the differences between gridded and inferred precipitation, we consider their spatial patterns in terms of distribution with elevation, and distribution topographically across the crest of the Sierra Nevada. Finally, we consider the patterns of implied ET from the gridded and inferred datasets across the range.

4.2. Precipitation multiplier prior and posterior distributions

The precipitation inferred from streamflow by the six FUSE model structures for Cherry-Eleanor is shown in Figure 2. The time series of the inferred precipitation ensemble shows substantial differences between FUSE structures, but also robustly reflects yearly variability in streamflow. In general, the ensemble of precipitation inferred from streamflow is greater than H10, similar or greater than the N15 ensemble, and contains the WRF precipitation. In the water year 2008 distribution (Figure 2e), the 95% confidence intervals of the inferred precipitation from each structure are shown, with the mean indicated by the marker. While the individual structures' intervals are about 100 mm wide, the range of the ensemble is almost 800 mm, showing that structural uncertainty in inferred precipitation is more substantial than the individual structures imply; this is consistent with the findings of Henn et al. (2015) and Henn et al. (2016a). The mean of the FUSE ensemble is also shown (1,332 mm); it is less than WRF but greater than H10 and N15.

A qualitative examination of this basin and others indicates that the posterior precipitation amounts generally fall within reasonable (95%) limits of the prior distributions. This suggests that the prior distributions are not grossly incompatible with the posterior

ACCEPTED MANUSCRIPT

distributions inferred from streamflow using the FUSE model structures. When this is the case, the specific choice of the prior distribution likely does not exert undue influence on the inferred precipitation. A sensitivity analysis of the inferred precipitation posterior (not shown) indicates that the results are only somewhat sensitive to the choice of prior distribution parameters, so long as the distribution is sufficiently wide as to span the posterior region. Thus, including WRF precipitation estimates is significant as it tends to increase the spread of the prior distribution. The posterior distributions of inferred precipitation largely reflect the best fit of the different model structures to streamflow.

Precipitation uncertainty (as measured by disagreement between the H10, N15 and WRF datasets) appears greatest in the central Sierra Nevada. When the difference between the datasets for each basin are normalized by the basin mean value and plotted spatially (not shown), greater relative uncertainty is seen in the Tuolumne, Merced and San Joaquin R. basins. Differences for these basins frequently exceed 20% of the mean, while in the southern Sierra Nevada differences are generally 10-15% or less, and the northern Sierra Nevada has intermediate values. However, the spatial pattern of uncertainty may be dependent on the choice of the particular precipitation datasets used in the comparison.

4.3. Comparing H10 precipitation and inferred precipitation in wet and dry years

For each of the 56 basins, we compile the inferred precipitation from the FUSE structures and calculate the mean of the FUSE ensemble for each basin-year. We exclude the basin-years in which model calibrations produced very poor fits to streamflow (streamflow Nash-Sutcliffe coefficient of -2 or less), or about 8% of all basin-years simulated. We then compare the mean inferred precipitation to H10 basin-mean precipitation for individual water years from 1950 to 2010.

ACCEPTED MANUSCRIPT

Figures 3 and 4 show this comparison for two water years (1983 and 1977). Water year 1983 was one of the wettest on record in the Sierra Nevada, with many gauges reporting over 2,000 mm of precipitation; H10 precipitation (Figure 3a) reflects the heavy precipitation that year, with most basins on the west slope of the Sierra Nevada north of 37°N averaging at least that much. Maximum accumulations are seen in the North Fork of the American R. and the South Fork of the Yuba R., as well in small adjacent basins. H10 precipitation generally decreases to the south along the west slope of the Sierra Nevada. In comparison, inferred precipitation (Figure 3b) shows a more spatially variable pattern: while precipitation of 2,500 mm or greater is seen in the Yuba and American basins, similarly large accumulations are seen in the basins in the Stanislaus, Tuolumne, San Joaquin, Kings and Kaweah drainages.

Water year 1983 streamflow (Figure 3c) shows a similarly spatially variable pattern. Of particular note are the strong gradients in streamflow seen over the central Sierra Nevada, with a local maxima over Cherry-Eleanor and Falls Crs., and much drier (>1,000 mm less streamflow) basins to the east in the Walker R. basin, and to the southwest in the lower Tuolumne R. basin. The spatial gradients are much less sharp in the H10 dataset than they are in streamflow, but are (not surprisingly) reflected in the precipitation inferred from streamflow.

To check H10 and inferred precipitation, we subtract observed streamflow from both datasets' basin-mean precipitation (Figures 3d and 3e). H10 precipitation minus streamflow is negative in several basins in water year 1983: Cherry-Eleanor (-175 mm), the North Fork of the Stanislaus R. (-16 mm) and Duncan Cr. (-75 mm). Several other basins have streamflow within about 100 mm of H10 precipitation, including the San Joaquin R. and its tributary Granite Cr. On the other hand, H10 precipitation minus streamflow is much greater for basins further from the crest of the Sierra Nevada. For example, the low-elevation Cosumnes and Mokelumne basins

ACCEPTED MANUSCRIPT

have H10 precipitation more than 800 mm greater than runoff. Inferred precipitation is greater than streamflow by more consistent amounts across the Sierra Nevada (Figure 3e), typically 400-800 mm, though local variability exists.

Finally, we plot the difference between H10 and inferred precipitation (Figure 3f), which highlights the different spatial patterns of precipitation from the two sources of information. Inferred precipitation is greater than H10 over most high-elevation basins, particularly in the central Sierra Nevada (Stanislaus, Tuolumne, San Joaquin, Kings and Kaweah basins). Precipitation inferred from streamflow is similar to or less than H10 for many of the lower-elevation basins, and for many of the basins east of the crest of the range.

The equivalent water year 1977 comparison (Figure 4) shows spatial patterns during an anomalously dry year (note different scale). Comparing Figures 3 and 4 shows that streamflow is on the order of 90% less in 1977 as compared to 1983. As a result, the absolute differences in streamflow and precipitation between basins in 1977 are relatively small, but as a fraction of water year totals (and considering the value of water in California in a drought year), they remain significant. For example, streamflow over 200 mm was observed in some central and northern basins (e.g., San Joaquin, Cherry-Eleanor, Falls Cr., the Stanislaus R. basins, and the Yuba R.), as compared to the southern portion of the range, where every basin west of the crest except the upper Kaweah R. had less than 200 mm of streamflow (Figure 4c). Streamflow was also strongly elevation-dependent, with lower-elevation basins producing less than 100 mm.

The spatial pattern of H10 precipitation in 1977 is relatively smooth, and the greatest basin-mean precipitation is in the south in the Kaweah R. basin (Figure 4a). In contrast, inferred precipitation reflects the northerly and high-elevation patterns of streamflow (Figure 4b). Thus, H10 precipitation minus streamflow tends to be greater in the south than in the north, while

ACCEPTED MANUSCRIPT

inferred precipitation minus streamflow is more spatially uniform (Figures 4d and 4e). The north-south difference is also highlighted in Figure 4f.

We next investigate the differences in the long-term mean spatial pattern between precipitation gauge-based gridded datasets and precipitation inferred from streamflow. To do so, we use the PRISM 1971-2000 precipitation climatology, which sets the long-term spatial pattern in the H10 dataset. We compare this against the mean annual inferred precipitation and streamflow, using all years in which streamflow is available for each basin (generally at least 30 for each basin). While the resulting map (Figure 5) does not compare consistent time periods, it is very similar to the map of H10 mean annual precipitation over the periods of streamflow data availability for each basin (not shown). This is because each basin has at least 30 years of streamflow data and samples close to the full range of yearly variability. The PRISM climatological precipitation pattern appears spatially smoother than the pattern of precipitation inferred from streamflow (Figures 5a-5b). The spatial pattern of average streamflow (Figure 5c) shows the same strong gradients between windward and leeward basins seen in single water years. While no basin has long-term PRISM (or H10) precipitation less than long-term streamflow (Figure 5d), streamflow does suggest very high runoff ratios based on PRISM precipitation for many windward, high-elevation basins (Figure 5f). Largely the same set of basins shows low values of PRISM climatological precipitation minus long-term streamflow as in the 1983 case (i.e., the San Joaquin, Cherry-Eleanor, and Stanislaus basins).

4.4. Comparison to other precipitation-gauge based gridded datasets

For comparison, we also plot the water year 1983 precipitation pattern of three other gridded datasets (N15, L15 and NLDAS-2) against streamflow (Figure 6). Qualitatively, the patterns of precipitation across the three datasets are similar, and are also similar to H10, though

ACCEPTED MANUSCRIPT

NLDAS-2 appears to have slightly less precipitation across the Sierra Nevada than the other datasets, and L15 appears to have somewhat more. In Figures 6d-6f, a set of basins shows low values of precipitation minus streamflow: the upper Kaweah R. basins, the San Joaquin R. and Granite Cr., Cherry-Eleanor and Falls Cr., the North Fork of the Stanislaus R. and Highland Cr., several of the small basins draining to Lake Tahoe, Duncan Cr., and the South Fork of the Yuba R. This set of basins is quite similar to those with low H10 precipitation minus streamflow (cf. Figure 3d), suggesting that the spatial patterns of precipitation across different gridded datasets are relatively similar.

4.5. Cross-range transects of precipitation and streamflow

To resolve the spatial patterns of precipitation and streamflow with respect to the topography of the Sierra Nevada, we plot them along two cross-range transects (Figure 7). The first transect begins in the Tuolumne R. basin on the west slope and travels northeast through the Walker R. basin, while the second begins in the Mokelumne R. basin, passes through the North Fork of the Stanislaus R. basin before crossing the range into the Carson R. basin. Given predominant cool-season winds out of the southwest (e.g., Lundquist et al., 2015), these transects pass from windward to leeward basins.

In the first transect (Figure 7b), the greatest streamflow is found near the top of the windward slope in the Cherry-Eleanor basin, while steep declines to both the southwest (Big Cr.), and in particular, the northeast (Walker R.) are seen. H10 precipitation generally places the greatest precipitation near the crest, but the maximum is likely too little given observed streamflow (Figure 7c). However, H10 precipitation appears compatible with streamflow and nearly matches inferred precipitation for Big Cr. and the Walker R. basins.

ACCEPTED MANUSCRIPT

In the second transect (Figure 7d), streamflow also reaches its peak on the high windward face of the range, in the North Fork of the Stanislaus R. basin. Similar to the first transect, H10 precipitation appears insufficient in this basin; H10 precipitation is slightly less than streamflow in water year 1983 (Figure 7e). Also similar to the first transect, the leeward basin (East Fork of the Carson R.) has much better agreement between H10 and inferred precipitation, but the lower-elevation windward basin (South Fork of the Mokelumne R.) has much greater H10 precipitation than inferred precipitation. In both transects, the higher-elevation windward basins have generally southwest-facing aspects; winds from this direction encounter a consistent upslope aspect and little upstream blocking, conditions favorable for orographic enhancement (Roe, 2005).

4.6. Interannual variability in spatial patterns of precipitation and streamflow

By considering multiple stream gauges in the Sierra Nevada, we can examine changes in the spatial pattern of streamflow and inferred precipitation from year to year. For this analysis, we select a subset of years and basins with complete records, so differences between years are due to changes in streamflow, and not due to changes in the set of basins. We select 1974-1987, a period in which 43 basins have complete streamflow records (Figure 8a). Within that set, we identify 15 basins on the west slope of the Sierra Nevada that are potentially underestimated by the gridded datasets based on the findings in the previous sections, and average these basins' streamflow and precipitation to represent the windward portions of the range. We identify 9 basins on the eastern side of the crest and average them to create a leeward group. Finally, we divide the basins into northern and southern groups (Figure 8a); the windward and leeward basins are also included in the appropriate northern and southern groups. With these indices of

ACCEPTED MANUSCRIPT

streamflow and precipitation, we can identify windward vs. leeward and north vs. south shifts between years.

In Figures 8b and 8c, we show windward-leeward and north-south ratios, respectively, of precipitation and streamflow. Streamflow is on average more than twice as great from the windward basins than from the leeward basins; however, the ratio varies from year to year, with 1978 in particular showing greater windward streamflow relative to the lee of the range (Figure 8b). This shift is reflected in the inferred precipitation, which has a lower mean windward-leeward ratio (~1.7), but generally follows the variability in streamflow. H10 windward-leeward precipitation ratios, however, are between 1.25 and 1.5, suggesting a weaker rain shadow, and show very little interannual variability. North-south ratios (Figure 8c) show substantial interannual variability, with precipitation and streamflow twice as large in the northern portion of the range compared to the south in some years, but near equal in others. Streamflow inferred precipitation and H10 precipitation track one another over this time period, though agreement is worse during the 1976 and 1977 drought years.

The annual difference between precipitation and streamflow in the Sierra Nevada implies the actual evapotranspiration (ET), as drainage to deep aquifers and changes in soil moisture storage are generally small compared to precipitation and streamflow. In some studies, ET has been estimated from the differences between basin-mean gridded precipitation and streamflow (Christensen et al., 2008; Lutz et al., 2010), and so we plot implied ET from the different basin groups under both H10 and inferred precipitation in Figures 8d and 8e. When considering windward-leeward differences, H10 precipitation implies that ET is greater in the leeward basins than the windward basins (Figure 8d). The difference between leeward and windward implied ET in H10 is variable, and appears larger in wetter water years (1978, 1982 and 1983). However,

ACCEPTED MANUSCRIPT

inferred precipitation implies that windward ET is greater than leeward ET, by a fairly constant margin. There is greater agreement between H10 and inferred precipitation regarding north-south differences in implied ET (Figure 8e): both datasets generally show greater ET in the northern basins, though in some years this is not the case for the H10 dataset. We discuss patterns of ET in more detail in section 5.

4.7. Trends in precipitation and streamflow

Using a subset of basins with at least 90% complete streamflow records over the study period (1950-2010), we calculate trends in the water year totals of observed streamflow, H10 basin-mean precipitation and inferred basin-mean precipitation. While there are fewer basins with sufficiently long and complete records to conduct the trend analysis, the spatial patterns of precipitation and streamflow trends can still be discerned (Figure 9). Trends in H10 precipitation show a strong north-south divide; the Kern and Kaweah basins in the south have positive precipitation trends, while all basins to the north have declines of 5-15%. In contrast, inferred precipitation (Figure 9b) shows increases in precipitation over the central Sierra Nevada in the Merced and San Joaquin basins, weaker trends in the southern portion of the domain, and decreases in the northern basins. In general, this follows from the observed streamflow trends, which are most positive over the central Sierra Nevada and are negative for all basins from the Mokelumne R. northward (Figure 9c). The trends in H10 precipitation, inferred precipitation and streamflow are all significantly correlated with latitude ($p < 0.10$, two-tailed Student's *t*-test). However, the differences between the H10 and inferred precipitation trends are greatest over the central Sierra Nevada (Figure 9d).

Thus, since 1950 streamflow appears to have increased over the Sierra Nevada from approximately Yosemite National Park southward, while the northern Sierra Nevada has seen

ACCEPTED MANUSCRIPT

declines in precipitation, streamflow and SWE. The H10 dataset appears to capture some, though not all, of these shifts in spatial patterns. While it does show the positive trends in precipitation in the southern Sierra Nevada, it does not capture the correct sign or magnitude of the increasing precipitation inferred over the central basins, in particular the San Joaquin, Merced and Walker basins. Trend uncertainties in gridded precipitation datasets were found to be common across different datasets in Henn et al. (2016b), this issue.

5. Discussion

5.1. Precipitation minus streamflow and ET estimates

The approach used here to infer precipitation from streamflow essentially forces basin water balance closure, and thus assumes that precipitation is the sum of observed streamflow and modeled actual ET, using the flexible precipitation input outlined in previous sections. Therefore, inferred precipitation represents a physically-based estimate of basin-mean precipitation given streamflow observations. Figure 2 and earlier studies using this framework make it clear that this formulation does produce uncertainties in the absolute amounts of inferred precipitation, due to uncertainties in hydrologic model structure and the parameterization of fluxes such as percolation and ET. The absolute inferred precipitation quantities presented here should be viewed with some care due to the uncertainty in inferred ET. However, year-to-year and basin-to-basin variability of inferred precipitation appear more robust than the absolute amount of inferred precipitation (Henn et al., 2015): while each FUSE model structure has a bias relative to the others, this bias is quite consistent across water years and basins. So we interpret the spatial pattern of inferred precipitation, as well as the yearly wet versus dry differences in inferred precipitation, as based on physical signals. In contrast, gridded precipitation products

ACCEPTED MANUSCRIPT

such as H10 leverage available precipitation observations to produce interpolated patterns, but interpolating gauge observations to a grid is a statistical process, not a physical one, and as such is subject to associated uncertainty.

Given these considerations, it is reasonable to check precipitation minus streamflow from both approaches against available observations and estimates of actual ET over the Sierra Nevada. However, measurements of ET over the Sierra Nevada are few, and uncertainty is high. Observational studies have estimated actual ET to be between 400 and 800 mm yr^{-1} at the point scale (Goulden et al., 2012; Ichii et al., 2009; Kurpius et al., 2003; Stephenson, 1998). Studies of forest cover and soils have shown that deep rooting allows trees and vegetation to access water stored in weathered bedrock (Bales et al., 2011; Rose et al., 2003), allowing for greater ET and maintenance of forests despite shallow (<1 m) soils and nearly precipitation-free summers in the Sierra Nevada's Mediterranean climate.

However, ET observations are exclusively made at the point scale in or over forest cover, and the extrapolation to spatially distributed, basin-mean ET has significant uncertainty. Goulden et al. (2012) and Goulden and Bales (2014) developed a relationship between the normalized difference vegetation index (NDVI) observed by the Moderate-Resolution Imaging Spectroradiometer (MODIS) and observations of actual ET at multiple flux towers in California, and used it to estimate basin-mean ET and elevational gradients of ET. Basin-scale studies can also infer ET through consideration of precipitation and streamflow, but both must be known well since ET is the remainder of two generally larger terms. (Our findings suggest that in many basins, gridded precipitation datasets may have too much uncertainty to apply this approach to reliably infer ET.) A two-year study in the forested Southern Sierra Critical Zone Observatory (SSCZO) in the Kings R. basin (Bales et al., 2011) estimated ET to be 760 mm yr^{-1}. This

ACCEPTED MANUSCRIPT

suggests that basin-mean ET is generally less than point estimates made in forests, presumably due to the areas of limited transpiration (i.e., rock, snow and grasses); a two-year water balance study of an above-treeline Kaweah basin found ET of 400 mm yr^{-1} (Kattelmann and Elder, 1991). The relationship between forest and basin-mean ET may depend on the fraction of forest cover in the basin.

In Figure 10 we consider preciptiation minus streamflow from the different precipitation data sources against observation-based estimates of ET over the Sierra Nevada. We plot long-term average precipitation, streamflow and precipitation minus streamflow against each basin's mean elevation in Figure 10a. The distribution of precipitation with elevation for H10 shows an increase at lower elevations, then a maximum at perhaps 2,000 m, followed by a slight decline above that elevation. The pattern for streamflow, and inferred precipitation, is more sensitive to elevation: streamflow increases rapidly from the lower elevation basins up to 2,000-2,500 m; there are few basins above this elevation. Inferred precipitation follows a similar pattern, but with a positive offset from streamflow. Precipitation minus streamflow (Figure 10b) for H10 shows a general decline with elevation, with the negative values noted above apparent at 1,800 m to 2,400 m in elevation. However, inferred precipitation minus streamflow is much less sensitive to elevation, with most values at all elevations between 400 and 800 mm yr^{-1}, presumably reflecting a relatively constant pattern of ET in the FUSE models across the basins.

Point observations of ET from the Sierra Nevada are plotted against elevation in Figure 10c, including estimates from Ameriflux tower sites (Ichii et al., 2009; Kurpius et al., 2003) and SSCZO flux towers and basin water balance (Bales et al., 2011; Goulden et al., 2012). We also apply the regression of ET against MODIS NDVI from Goulden et al. (2012) to estimate basin-mean ET for each of the streamflow basin (gray circles), using the mean MODIS NDVI from

ACCEPTED MANUSCRIPT

water year 2003. Collectively, these observations show that ET likely peaks in the middle elevations (1,000-2,000 m), with declines at higher and lower elevations. We can interpret this difference given arguments about ET over the elevation range of the Sierra Nevada. While higher, colder basin have shorter growing seasons and less PET, they also have greater water availability compared to lower-elevation basins due to greater precipitation. Given the Sierra Nevada's arid summers and shallow soils, actual ET is generally driven more by water availability than PET, i.e., the climate is generally more water-limited at all but the highest elevations. The resulting tradeoffs appear to favor the greatest actual ET in the middle elevations, particularly on the windward side (Christensen et al., 2008; Goulden et al., 2012), which is also where the greatest forest cover is located (Stephenson, 1998). The NDVI-based approach in particular suggests that there is less ET (<400 mm yr^{-1}) in high-elevation and leeward basins. However, because Goulden et al. (2012) based their regression on flux towers that are located primarily at sites at lower elevations and in more arid regions than the high Sierra Nevada, they note that it may underestimate ET in energy-limited alpine areas where NDVI is not a strong indicator of water availability. For example, studies of evaporation and sublimation from the snowpack in the Sierra Nevada have estimated it to be from near zero to 300-400 mm yr^{-1}, the substantial uncertainty is due to a lack of direct measurements (Leydecker and Melack, 1999). Thus, the NDVI-based estimates are probably best considered as a lower bound of ET in the higher-elevation basins.

In the lower row of Figure 10, we plot the spatial pattern of precipitation minus streamflow from H10 (d), inferred precipitation minus streamflow (e) and ET from the NDVI-based regression (f). The spatial patterns exhibit significant differences, with H10 and inferred precipitation showing greater precipitation minus streamflow than NDVI-based ET over many of

ACCEPTED MANUSCRIPT

the higher-elevation basins in the central and southern Sierra Nevada as well as east of the crest. The different estimates also suggest that the precipitation inferred from streamflow using the FUSE models may overestimate high-elevation ET in basins with little vegetative cover. However, the NDVI-based approach does suggest that basins of similar elevation and forest cover (e.g., the Tuolumne and Merced basins in the central portion of the range) have similar amounts of ET. While the NDVI-based ET amounts are less than inferred precipitation minus streamflow, these spatial patterns of variability (Figures 10e-f) are more similar than the H10 pattern (Figure 10d). The NDVI-based approach does not support aspects of the H10 dataset in which certain basins (e.g., Cherry-Eleanor) have much less precipitation minus streamflow than basins of similar elevation, or that ET is greater on the leeward slope of the Sierra Nevada as compared to the windward slope. We interpret those features of the H10 dataset to be more likely due to underestimation of precipitation in grid interpolation.

5.2. Estimation of regional hydro-climatology from streamflow data

These findings contribute to our understanding of regional orographically-driven precipitation patterns. The basins with the highest rates of inferred precipitation tend to follow certain orientations, specifically facing southwest on ridges that protrude west from the main crest of the Sierra Nevada. This provides information about where upslope flow must occur during winter storms, and may aid in validation of precipitation forecast models. It also highlights the challenges in using interpolation approaches to map spatial patterns of precipitation over topography.

The maps (Figures 3-6) and transect plots (Figures 7) of the difference between gridded and inferred precipitation yield several consistent spatial patterns. First, the likely underestimation of precipitation by H10 occurs over higher-elevation windward basins with

ACCEPTED MANUSCRIPT

generally southwest aspect (Duncan Cr., Cole Cr., the North Fork of the Stanislaus R. and Highland Cr., Cherry-Eleanor and Falls Cr., Granite Cr. and the San Joaquin R., and the Marble Fork and main stem of the Kaweah R.). Lower-elevation basins on the west slope, basins in the far southern Sierra Nevada, and basins east of the crest generally show better agreement, or even potential overestimation by H10. This pattern is illustrated in Figures 7, which shows the greatest disagreement occurring in relatively high-elevation windward basins. The apparent enhancement and mainly southwestern aspect of these basins agrees with findings that the predominant moisture transport into the Sierra Nevada is from low-level southwesterly winds during cool-season storms (e.g., Lundquist et al., 2015).

Given that these findings are essentially the result of basins with higher streamflow than others at similar elevation and latitude (Figures 3-5, 7 and 10), the reliability of the streamflow observations deserves consideration. Streamflow measurements are subject to uncertainty in the rating curve and depth measurements, which produce instantaneous errors in flow measurement, and may lead to biases if not validated with reliable instream flow measurements. However, we consider the likelihood of large, long-term biases in streamflow data to be relatively small, assuming that the gauges are well-maintained and that the USGS considers the records to be of reasonable quality. It is possible that any individual gauge has a substantial bias; however, the patterns of streamflow seen in Figures 3-5 appear to be spatially coherent. They exhibit as a generally north-to-south, wet-to-dry pattern, and appears to favor southwest-facing basins with no upstream blocking. The apparent enhancement in these topographically favored basins is supported by theoretical and observational studies of relatively small-scale precipitation patterns in complex terrain (Anders et al., 2007; Frei and Schar, 1998; Minder et al., 2008; Roe, 2005): mountainous areas receiving the greatest precipitation generally are those in which prevailing

ACCEPTED MANUSCRIPT

moisture-bearing winds are forced upslope due to favorable topographic aspect. These factors suggest that the long-term streamflow measurements are relatively robust.

The patterns appear also fairly consistent in time across the water years surveyed and in the long-term average pattern. Thus, it suggests that there may be low bias in the spatial mean pattern of precipitation in the gridded datasets, which in H10 (and most similar datasets) is set to match PRISM precipitation climatology. Other PRISM-based gridded datasets (L15, NLDAS-2) show relatively similar patterns of potential underestimation (Figure 6), suggesting that this climatology may be a source of the underestimation. PRISM uses a detailed topographic interpolation scheme that reflects the spatially-variable relationship between precipitation and elevation on slopes of different aspect and of different exposure to prevailing moisture sources. However, it ultimately relies on gauge observations (as well as April 1 snow course observations in some cases where gauges are sparse in the Sierra Nevada) to obtain the elevation-precipitation relationship. If there are few or no gauges on certain preferential slopes where air parcels are forced upward due to aspect and topographic convergence (Roe, 2005), it will be difficult for the regression to capture these local maxima. A companion analysis of differences between gridded precipitation datasets suggests the central and southern Sierra Nevada have sufficiently few gauges and the topographic complexity necessary to produce substantial gridding uncertainty (Henn et al., 2016b, this issue). As a result, topographic interpolation may underestimate precipitation for basins in these areas.

Because many datasets use PRISM climatology to establish the mean spatial pattern of precipitation over complex terrain, the potential biases seen in Figures 3-6 do not just apply to the H10 dataset, but to a broader array of gridded precipitation products. In fact, even the gridded precipitation dataset that does not rely on PRISM (N15) shows a relatively similar spatial pattern

ACCEPTED MANUSCRIPT

of precipitation. Given these findings, it appears that underestimation of local precipitation maxima in complex terrain could be a widespread feature of gridded precipitation datasets.

In contrast, we note that WRF precipitation may better represent precipitation in some of the basins with high observed streamflow. As seen in the Cherry-Eleanor example and in Sierra-wide maps of water year total precipitation (Figure 2), the WRF simulation has greater precipitation than the gridded datasets, particularly for northern and high-elevation windward basins. WRF patterns of precipitation minus streamflow did not show low values in the basins where underestimation is likely in H10 and the other gridded datasets. This suggests that WRF is capturing the dynamics of local orographic enhancement and may better reproduce local maxima in streamflow. Some studies argue that WRF precipitation over mountains is generally too high (Caldwell et al., 2009; Grubišić et al., 2005), and the WRF data shown here do produce high values of precipitation minus streamflow overall. But given that gridded precipitation datasets are usually used to evaluate WRF, it appears possible that the apparent wet biases in WRF in some areas actually may be dry biases in the gridded products.

6. Conclusions

From the comparison between streamflow from 56 long-term, largely unimpaired Sierra Nevada stream gauges, gridded precipitation, and precipitation inferred from streamflow, over water years 1950 to 2010, we draw the following conclusions:

1) There are differences between the mean spatial pattern of gridded precipitation in H10 (and other gridded datasets, most of which are set by PRISM climatology) and the spatial pattern of precipitation inferred from streamflow. In particular, streamflow implies

ACCEPTED MANUSCRIPT

greater precipitation in higher-elevation, southwest-facing basins than is seen in H10 and other gridded datasets.

2) The spatial and temporal variability of precipitation inferred from streamflow (e.g., precipitation gradients over the crest of the Sierra Nevada) is higher than in H10 gridded precipitation. While absolute uncertainties in inferred precipitation are relatively high, the spatial patterns are relatively robust, such that the gradients in streamflow also likely represent gradients in the precipitation pattern.
3) The relationship between implied actual ET (precipitation minus streamflow) across the crest of the Sierra Nevada is different between the gridded precipitation dataset and inferred precipitation: H10 implies actual ET is similar or greater in a set of basins to the lee of the crest relative to a set on the windward side, while implied actual ET is greater on the windward side with inferred precipitation.
4) 1950-2010 trends in inferred precipitation show increases over the central and southern Sierra Nevada; in contrast, H10 precipitation trends show declines over the central Sierra Nevada.

Acknowledgements

BH, JDL and MH received support from NSF Grant No. EAR-1344595. AJN acknowledges support from the US Army Corps of Engineers Climate Preparedness and Resilience Program and the US Bureau of Reclamation. Gridded H10 were downloaded from the Columbia Basin Climate Change Scenarios Project website at http://warm.atmos.washington.edu/2860; these materials were produced by the Climate Impacts Group at the University of Washington in collaboration with the WA State Department of

ACCEPTED MANUSCRIPT

Ecology, Bonneville Power Administration, Northwest Power and Conservation Council, Oregon Water Resources Department, and the B.C. Ministry of the Environment. This work was facilitated though the use of advanced computational, storage, and networking infrastructure provided by the Hyak supercomputer system at the University of Washington; we thank Bart Nijssen and the University of Washington Computational Hydrology Group, and the University of Washington Student Technology Fund, for providing additional computational resources. We thank Adrian Dobra for guidance on Bayesian statistics, and members of the University of Washington Mountain Hydrology Research Group for valuable feedback and reviews.

ACCEPTED MANUSCRIPT

ACCEPTED MANUSCRIPT

7. Tables

Table 1. Sierra Nevada unimpaired streamflow gauge and basin information.

USGS Gauge Number	USGS Gauge Name	Watershed	Latitude	Longitude	Gauge Elevation [m]	Basin Mean Elevation [m]	Basin Peak Elevation [m]	Basin Area [km^2]	Starts	Ends	Years	HCDN	Quality	Notes
10270872	MF BISHOP C BL LK SABRINA NR BISHOP CA	Owens	37°12''50"	118°36''34"	2,762	3,457	4,212	43.6	1990	-	26	Y	-	Regulation by Lake Sabrina (USGS station 10270870); mass balance correction applied to flow record
10276001	COMBINED Q BIG PINE C & GIROUX DITCH CA		37°08''42"	118°18''52"	1,372	2,997	4,336	100.5	1931	1978	48	N	Poor	Includes both river and diversion
10281800	INDEPENDENCE C BL PINYON C NR INDEPENDENCE CA		36°46''43"	118°15''49"	1,616	2,996	4,130	31.3	1924	1978	55	N	Poor	No diversions or regulations
10286001	COTTONWOOD C NR OLANCHA CA.+ PH CA		36°26''20"	118°04''48"	1,421	3,058	4,263	103.8	1907	1978	72	N	Poor	Includes both river and diversion
10291500	BUCKEYE CK NR BRIDGEPORT, CA	Walker	38°14''20"	119°19''30"	2,104	2,804	3,612	114.1	1954	-	62	Y	Good	No regulation or diversion above station; WYs 1980-1995 missing
10295500	L WALKER RV NR BRIDGEPORT, CA		38°21''39"	119°26''38"	2,070	2,647	3,527	163.0	1945	2008	64	Y	Good	Small diversions above stations; WYs 1987-1995 missing

ACCEPTED MANUSCRIPT

ACCEPTED MANUSCRIPT

10296000	W WALKER R BL L WALKER R NR CO		38°22''47"	119°26''57"	2,010	2,696	3,577	469.1	1939	-	77	Y	Fair	Small diversions upstream; slight regulation by Poore Lake
10296500	W WALKER R NR COLEVILLE, CA		38°30''48"	119°26''56"	1,683	2,624	3,577	632.0	1958	-	58	Y	Fair	Small diversions upstream; slight regulation by Poore Lake
10308200	E FK CARSON RV BLW MARKLEEVILLE CK NR MARKLEEVILLE	Carson	38°42''53"	119°45''50"	1,646	2,412	3,489	717.2	1961	-	52	Y	Fair	Small diversions upstream; slight regulation by small reservoirs
10310000	W F CARSON R AT WOODFORDS, CA		38°46''11"	119°49''58"	1,754	2,458	3,309	170.0	1939	-	74	Y	Fair	Small diversions upstream; small regulation upstream
10310400	DAGGETT CK NR GENOA, NV		38°57''52"	119°50''57"	1,555	2,220	2,915	10.1	1972	-	39	Y	Good	No diversions above station; WYs 1984-1988 missing
10336660	BLACKWOOD CREEK NR TAHOE CITY	Tahoe	39°06''27"	120°09''40"	1,901	2,217	2,704	29.6	1961	-	55	Y	Fair	No known diversion or regulation; ice error in winter
10336676	WARD C AT HWY 89 NR TAHOE PINES CA		39°07''56"	120°09''24"	1,899	2,222	2,704	24.9	1973	-	43	Y	Good	Minor diversions upstream
10336780	TROUT CREEK NR TAHOE VALLEY CA		38°55''12"	119°58''17"	1,903	2,426	3,318	93.9	1961	-	55	Y	Good	Minor diversions upstream; ice error in winter
10343500	SAGEHEN CREEK NR TRUCKEE CALIF		39°25''54"	120°14''13"	1,927	2,164	2,656	27.6	1954	-	62	Y	Good	No storage or diversion upstream

ACCEPTED MANUSCRIPT

ACCEPTED MANUSCRIPT

11186001	COMBINED FLOW OF KERN R AND KERN R NO 3 CA	Kern	35°56''43"	118°28''36"	1,104	2,632	4,403	2,190.2	1911	-	104	Y	-	Includes both river and SCE diversion
11187000	KERN RIVER AT KERNVILLE CALIF		35°45''16"	118°25''21"	799	2,495	4,403	2,610.5	1954	1993	40	N	Good	A few small diversions for irrigation upstream from station
11189500	SF KERN R NR ONYX CALIF		35°44''15"	118°10''22"	884	2,357	3,691	1,371.0	1946	-	66	Y	-	<15 cfs diversions upstream
11199500	WHITE R NR DUCOR CA	Tulare	35°48''36"	118°55''03"	218	744	2,526	234.9	1972	2005	33	N	Good	No regulation or diversion
11202001	NF OF MF TULE R NR SPRINGVILLE CALIF (TOTAL FLOW)		36°10''29"	118°41''41"	890	2,057	3,116	101.4	1940	-	72	Y	-	Includes both river and PG&E diversion
11204500	SF TULE R NR SUCCESS CA		36°02''33"	118°51''24"	235	1,238	2,831	285.2	1931	1990	60	N	-	
11206501	MF KAWEAH R NR POTWISHA CAMP CALIF (TOTAL FLOW)	Kaweah	36°30''47"	118°47''27"	640	2,287	3,826	266.1	1950	2002	53	N	-	Includes both river and SCE diversion
11208001	MARBLE FK KAWEAH AT POTWISHA CP CALIF TOTAL FLOW		36°31''19"	118°47''54"	674	2,403	3,494	132.7	1950	2002	53	N	-	Includes both river and SCE diversion
11208731	COMBINED FLOW EF KAWEAH R NR THREE RIVERS CA		36°27''05"	118°47''15"	762	2,315	3,791	222.5	1957	2002	29	N	-	Includes both river and SCE diversion; WYs 1978-1993 missing

ACCEPTED MANUSCRIPT

ACCEPTED MANUSCRIPT

11209900	KAWEAH RIVER AT THREE RIVERS CALIF		36°26''38"	118°54''09"	247	1,894	3,826	1,085.3	1959	1990	42	N	Good	Diversions of up to 200 acre-ft/yr upstream
11210100	SOUTH FORK KAWEAH RIVER AT THREE RIVERS, CALIF.		36°25''00"	118°54''48"	246	1,578	3,472	230.3	1959	1990	42	N	Good	Several small diversions upstream from station for irrigation
11213500	KINGS RIVER AB NF NR TRIMMER CALIF	Kings	36°51''48"	119°07''24"	305	2,621	4,338	2,463.4	1932	1982	51	N	Good	No diversions or regulations
11218501	COMBINED FLOW KINGS R BL N F & KINGS R PP CA		36°52''29"	119°08''27"	287	2,551	4,338	3,471.5	1953	1993	41	n	Good	NF Kings portion regulated post-1957; includes both river and powerplant flow
11221700	MILL CREEK NEAR PIEDRA CALIF		36°49''07"	119°20''27"	168	782	2,197	328.3	1958	1994	37	N	Good	Some small diversions upstream from station for irrigation
11226500	SAN JOAQUIN R AT MILLER CROSSING CALIF	San Joaquin	37°30''38"	119°11''47"	1,393	2,781	4,009	650.5	1922	1991	47	N	-	WYs 1929-1951 missing
11228500	GRANITE C NR CATTLE MOUNTAIN CA		37°31''36"	119°15''28"	2,073	2,709	3,539	123.9	1966	1986	21	N	-	No diversion from station
11230500	BEAR CR NR LAKE T.A.EDISON CALIF		37°20''22"	118°58''21"	2,246	3,244	4,177	136.3	1922	-	94	Y	-	No storage or diversion upstream of station
11237500	PITMAN C BL TAMARACK CREEK CALIF		37°11''55"	119°12''46"	2,140	2,436	3,002	59.9	1928	-	88	Y	-	No diversion upstream from station

ACCEPTED MANUSCRIPT

ACCEPTED MANUSCRIPT

11264500	MERCED R AT HAPPY ISLES BRIDGE NR YOSEMITE CALIF	Merced	37°43''53"	119°33''29"	1,225	2,747	3,980	469.8	1916	-	100	Y	Good	Up to 5 cfs diverted upstream from station (prior to 1986)
11266500	MERCED RIVER AT POHONO BRIDGE NEAR YOSEMITE, CAL		37°43''01"	119°39''55"	1,177	2,577	3,980	834.5	1916	-	100	Y	Good	Small historical diversions between Happy Isles and Pohono
11275000	FALLS C NR HETCH HETCHY CA	Tuolumne	37°58''15"	119°45''48"	1,631	2,599	3,545	119.4	1916	1983	68	N	Good	No regulation or diversion
-	TUOLUMNE R A HETCH HETCHY		37°58''15"	119°47''18"	1,067	2,723	3,984	1,172.8	1970	-	46	Y	Fair	HHWP full natural flows
-	CHERRY CR A CHERRY LAKE + ELEANOR CR A LAKE ELEANOR		37°58''29"	119°54''36"	1,357	2,344	3,275	485.7	1974	2013	40	Y	Fair	HHWP full natural flows; includes flow of Eleanor basin, connected by tunnel
11281000	SF TUOLUMNE RIVER NR OAKLAND RECREATION CAMP CAL		37°49''18"	120°00''43"	854	1,692	2,813	225.6	1924	-	85	N	Good	No diversion, small regulation upstream; USGS record ends in 2002; reappears on CDEC in 1/2009 as STO
11282000	MIDDLE TUOLUMNE R AT OAKLAND RECREATION CAMP CAL		37°49''42"	120°00''38"	854	1,869	2,930	165.1	1917	-	92	N	Good	No regulation, small diversions; USGS record ends in 2002; reappears on CDEC in 1/2009 as MTO
11283500	CLAVEY RIVER NEAR BUCK MEADOWS, CALIF.		37°54''02"	120°04''15"	724	1,802	2,825	378.2	1960	1994	35	N	Good	No storage or diversion upstream of station; WYs 1984-1986

ACCEPTED MANUSCRIPT

ACCEPTED MANUSCRIPT

														missing
11284400	BIG C AB WHITES GULCH NR GROVELAND CA		37°50''31"	120°11''02"	781	961	1,210	41.7	1970	-	46	Y	Good	No storage or diversion
11292000	MF STANISLAUS R AT KENNEDY MDWS NR DARDANELLE CA	Stanislaus	38°17''51"	119°44''25"	1,929	2,725	3,520	123.6	1938	-	78	Y	-	No diversion, but higher summer low flows due to releases from Relief Reservoir
11292500	CLARK FORK STANISLAUS RIVER NEAR DARDANELLE, CAL		38°21''50"	119°52''13"	1,679	2,497	3,428	174.8	1951	1994	44	N	Good	No regulation or diversion upstream
11293500	NF STANISLAUS R BL SILVER CREEK CALIF		38°26''22"	120°00''53"	2,036	2,303	2,868	74.4	1953	1987	35	N	-	Low/medium flows regulated by Union/Utica/Alpine reservoirs; no diversions
11294000	HIGHLAND C BL SPICER MEADOWS RES CALIF		38°23''35"	119°59''53"	1,933	2,343	3,024	119.8	1953	1987	60	Y	-	
11315000	COLE C NR SALT SPRINGS DAM CALIF	Mokelumne	38°31''09"	120°12''42"	1,805	2,260	2,842	54.1	1928	-	85	Y	-	Occasional pumping upstream from station for summer homes
11316800	FOREST CREEK NEAR WILSEYVILLE, CALIF.		38°24''12"	120°26''45"	899	1,419	2,108	54.6	1960	-	53	Y	-	No regulation, minor diversions upstream for irrigation and domestic use

ACCEPTED MANUSCRIPT

ACCEPTED MANUSCRIPT

11317000	MF MOKELUMNE R A WEST POINT CA		38°23''23"	120°31''32"	747	1,336	2,248	178.0	1911	-	105	Y	-	Up to 10 cfs diversion from this basin to SF Mokelumne; slight regulation by Schaads Res. since 1940; other small diversions
11318500	SF MOKELUMNE R NR WEST POINT CA		38°22''06"	120°32''40"	595	1,250	2,113	194.6	1933	-	82	Y	-	Up to 10 cfs diversion from MF Mokelumne to this basin; up to 9 cfs diversion out of basin to Jeff Davis Res.
11335000	COSUMNES R A MICHIGAN BAR CA		38°30''01"	121°02''39"	51	934	2,357	1,387.3	1907	-	109	Y	Good	Regulation and diversion by Jenkinson Lake, some transfers out of basin
11414000	SOUTH YUBA RIVER NEAR CISCO, CALIF.	Yuba	39°19''17"	120°33''48"	1,683	2,106	2,754	140.3	1943	1994	52	N	Fair	Low flow regulated by several small PG&E reservoirs
11427000	NF AMERICAN R AT NORTH FORK DAM CALIF	American	38°56''10"	121°01''22"	218	1,329	2,736	884.0	1942	-	74	Y	Good	Minor regulation by Lake Clementine, Big Reservoir, Lake Valley Reservoir; diversion into Bear River basin; minor effect on natural flows
11427700	DUNCAN CREEK NR FRENCH MEADOWS CALIF		39°08''09"	120°28''39"	1,607	1,950	2,263	25.6	1961	-	55	Y	-	No regulation or diversion upstream from station

ACCEPTED MANUSCRIPT

ACCEPTED MANUSCRIPT

11431800	PILOT CREEK ABOVE STUMPY MEADOWS RESERVOIR, CALI		38°53''41"	120°34''02"	1,305	1,568	1,883	30.2	1960	2008	48	N	Good	No regulation or diversion upstream from station
11440000	ALDER C NR WHITEHALL TOTAL FLOW CA		38°45''19"	120°22''17"	1,171	1,801	2,274	57.2	1923	1981	59	N	-	Includes flow diverted into pipeline

ACCEPTED MANUSCRIPT

ACCEPTED MANUSCRIPT

8. Figures

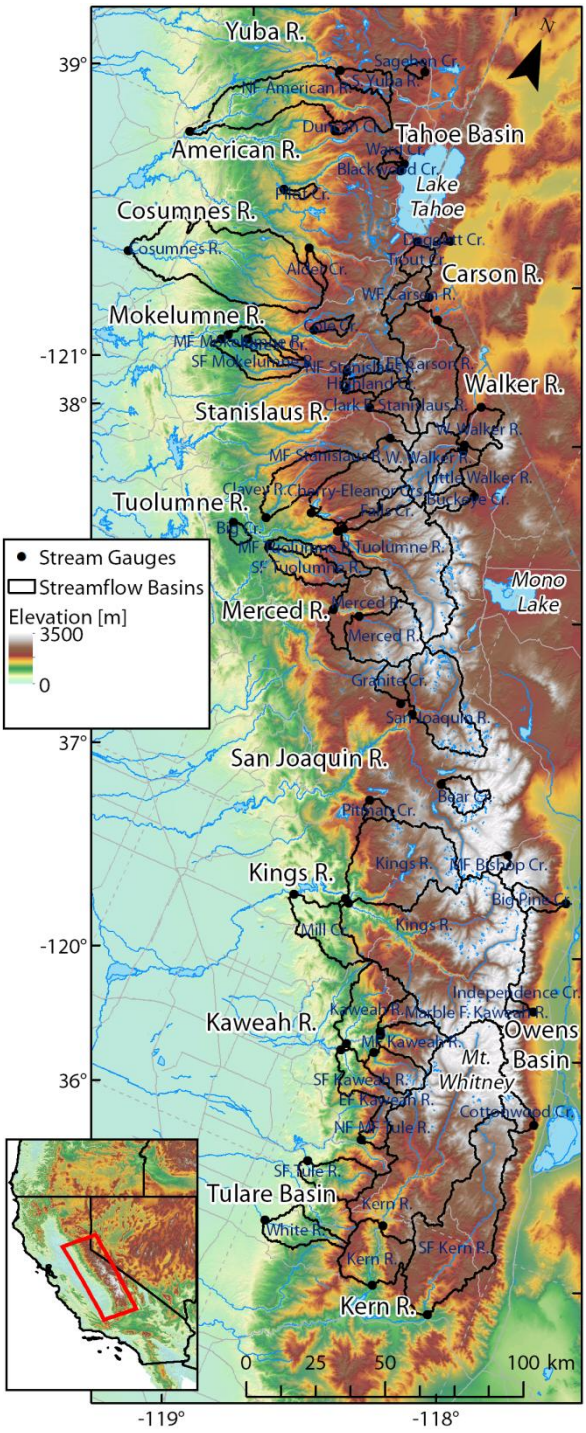


Figure 1. Topographic map of the Sierra Nevada showing streamflow basins used in this study; major drainages are labeled.

ACCEPTED MANUSCRIPT

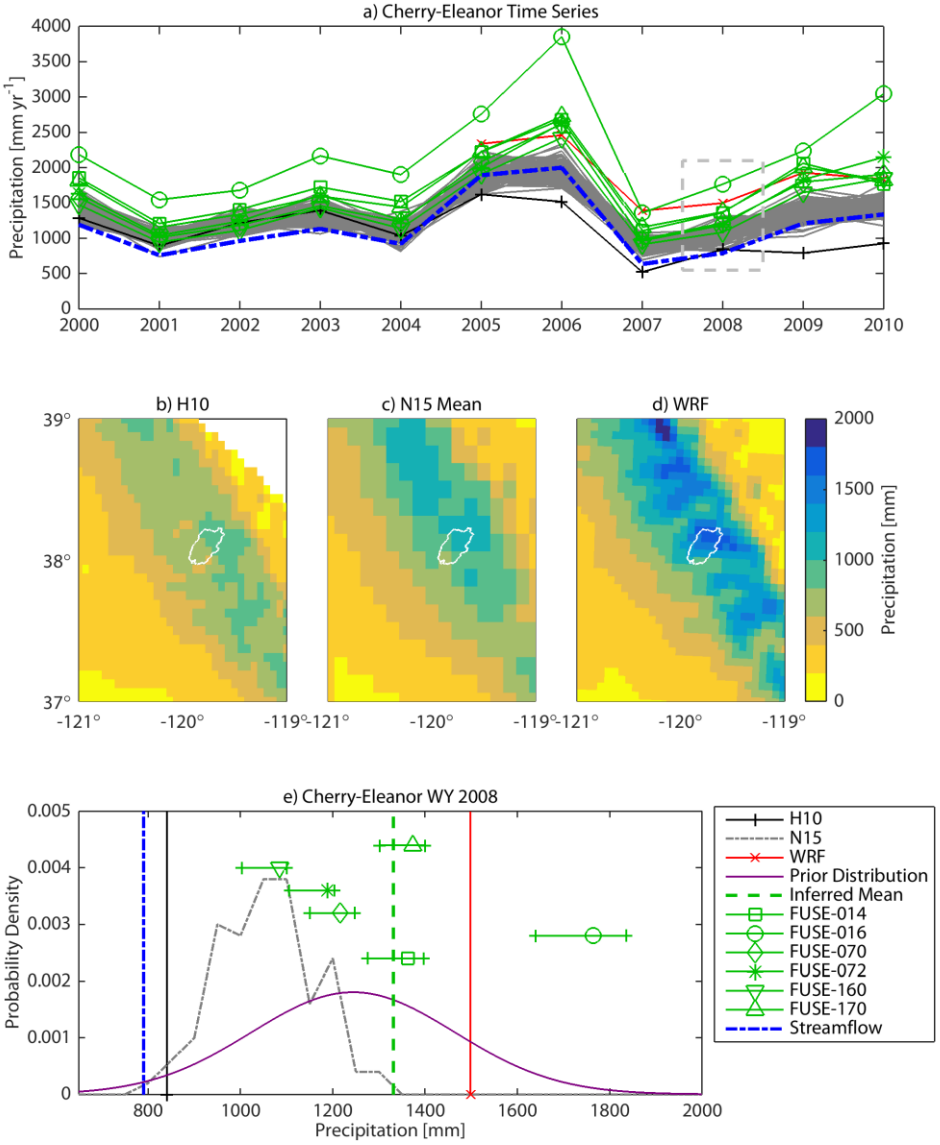


Figure 2. Comparison of prior and posterior precipitation distributions for the Cherry-Eleanor basin. a) Time series of water year total precipitation from H10, N15 and WRF, along with streamflow, and the precipitation inferred from streamflow (FUSE structures). b)-d) Maps of water year 2008 total precipitation from each data source over the portion of the Sierra Nevada around Cherry-Eleanor basin (shown in white outline). e) Probability distributions of precipitation for Cherry-Eleanor in water year 2008, showing fixed precipitation dataset values, the prior distribution that is based on the datasets, and the posterior distribution of precipitation from the six FUSE structures. Vertical axis is normalized so that distributions sum to 1; inferred precipitation is shown as credible intervals with the symbol indicating the mean value. FUSE intervals are plotted at arbitrary vertical positions to clearly show their horizontal distributions.

ACCEPTED MANUSCRIPT

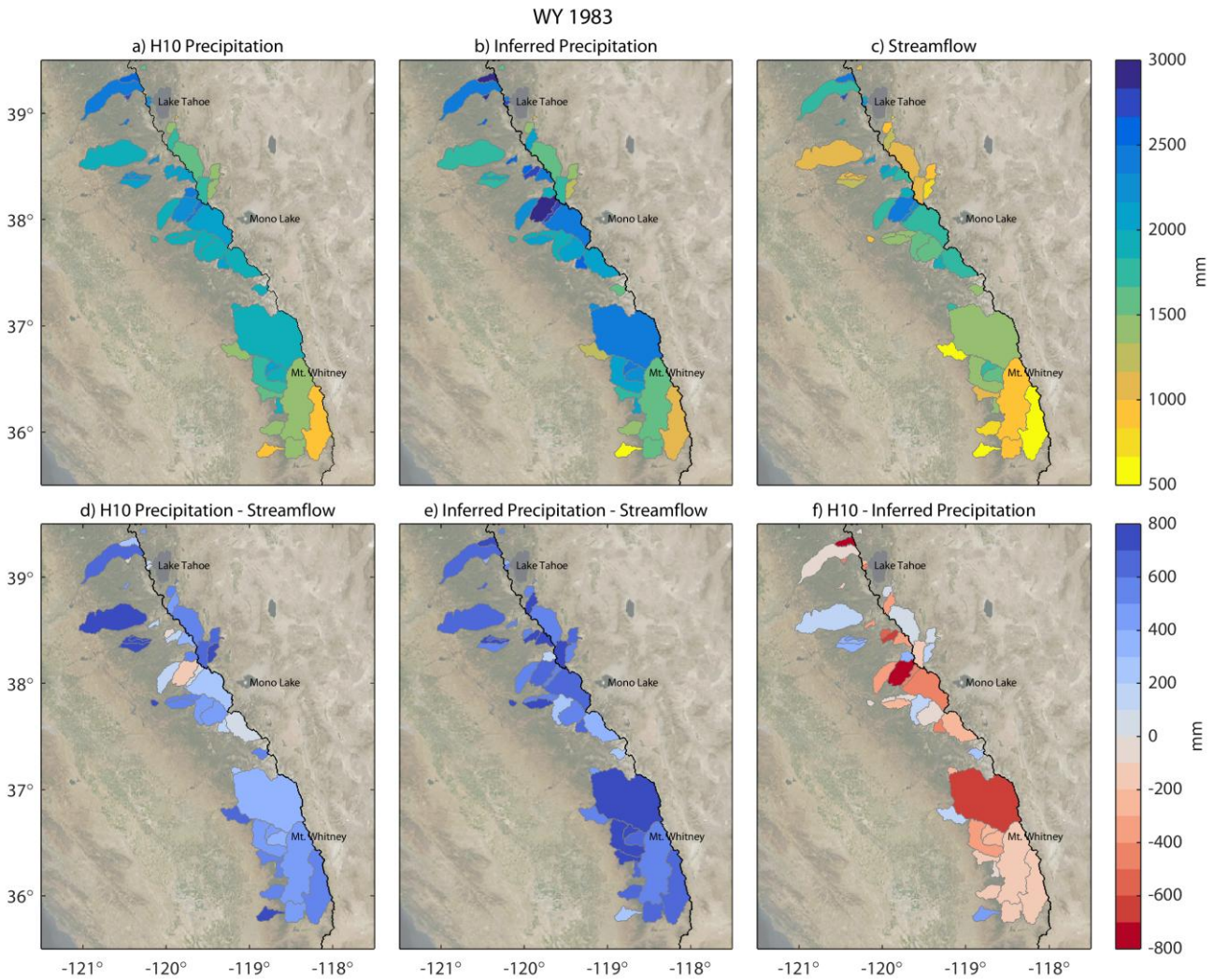


Figure 3. Basin-mean precipitation for water year 1983 from H10 (a) and from inferred precipitation (b). c) Water year streamflow totals. d) and e): Basin-mean differences between H10 and streamflow, and inferred precipitation and streamflow, respectively. f) Basin-mean differences between H10 and inferred precipitation. The crest of the Sierra Nevada is shown in black; background from LANCE Rapid Response MODIS images (http://lance-modis.eosdis.nasa.gov/).

ACCEPTED MANUSCRIPT

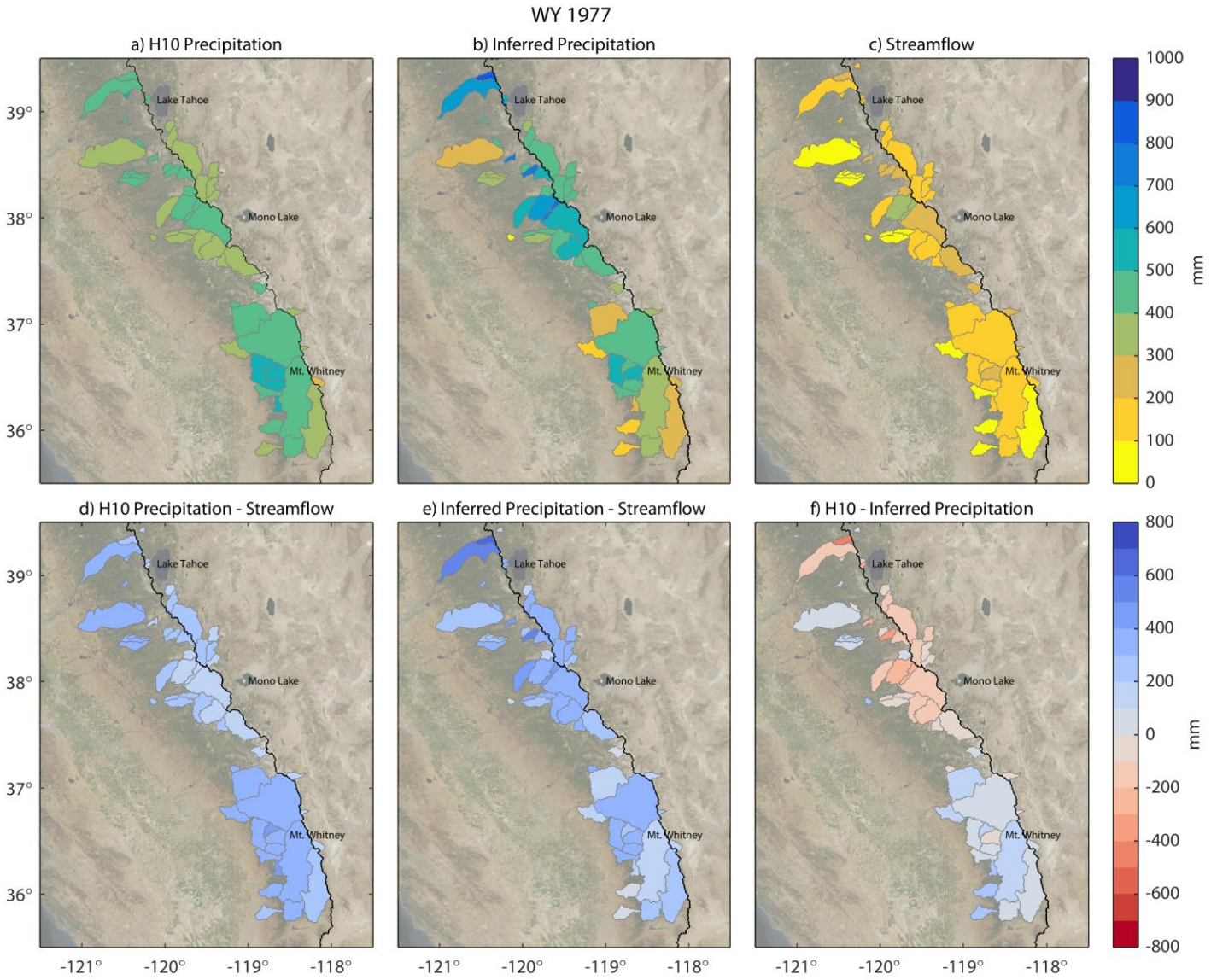
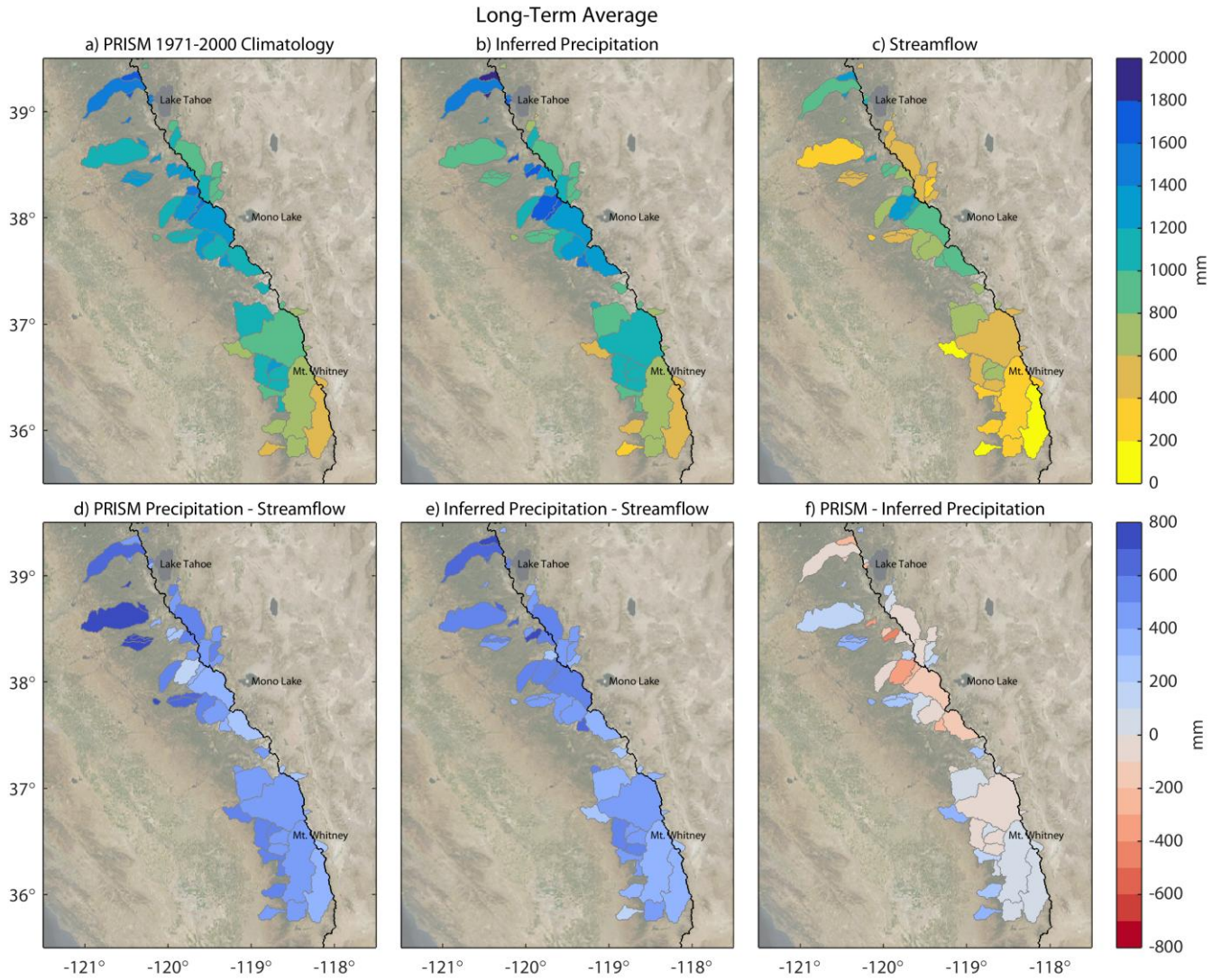


Figure 4. Same as Figure 3, but for water year 1977. Note different color scale from Figure 3.

ACCEPTED MANUSCRIPT



ACCEP

ACCEPTED MANUSCRIPT

Figure 5. Comparison of PRISM precipitation climatology (a) against long-term average precipitation inferred from streamflow (b), streamflow (c). d) PRISM precipitation climatology minus streamflow. e) Long-term average inferred precipitation minus streamflow. f) Difference between PRISM precipitation climatology and long-term average inferred precipitation.

ACCEPTED MANUSCRIPT

ACCEPTED MANUSCRIPT

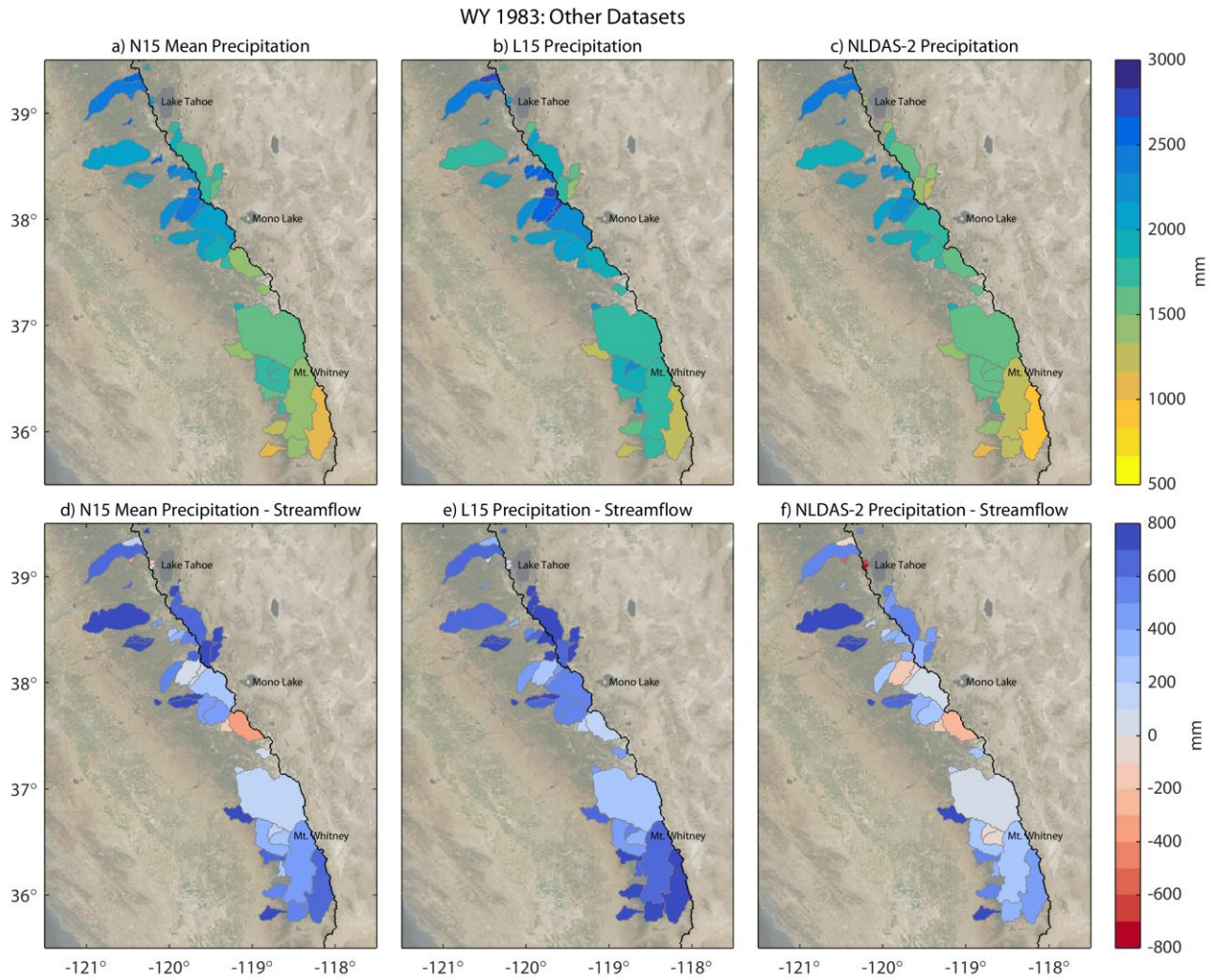


Figure 6. Top row: water year 1983 basin-mean precipitation for three other gridded datasets (N15, L15 and NLDAS-2). Bottom row: precipitation minus streamflow for each of the same datasets.

ACCEPTED

ACCEPTED MANUSCRIPT

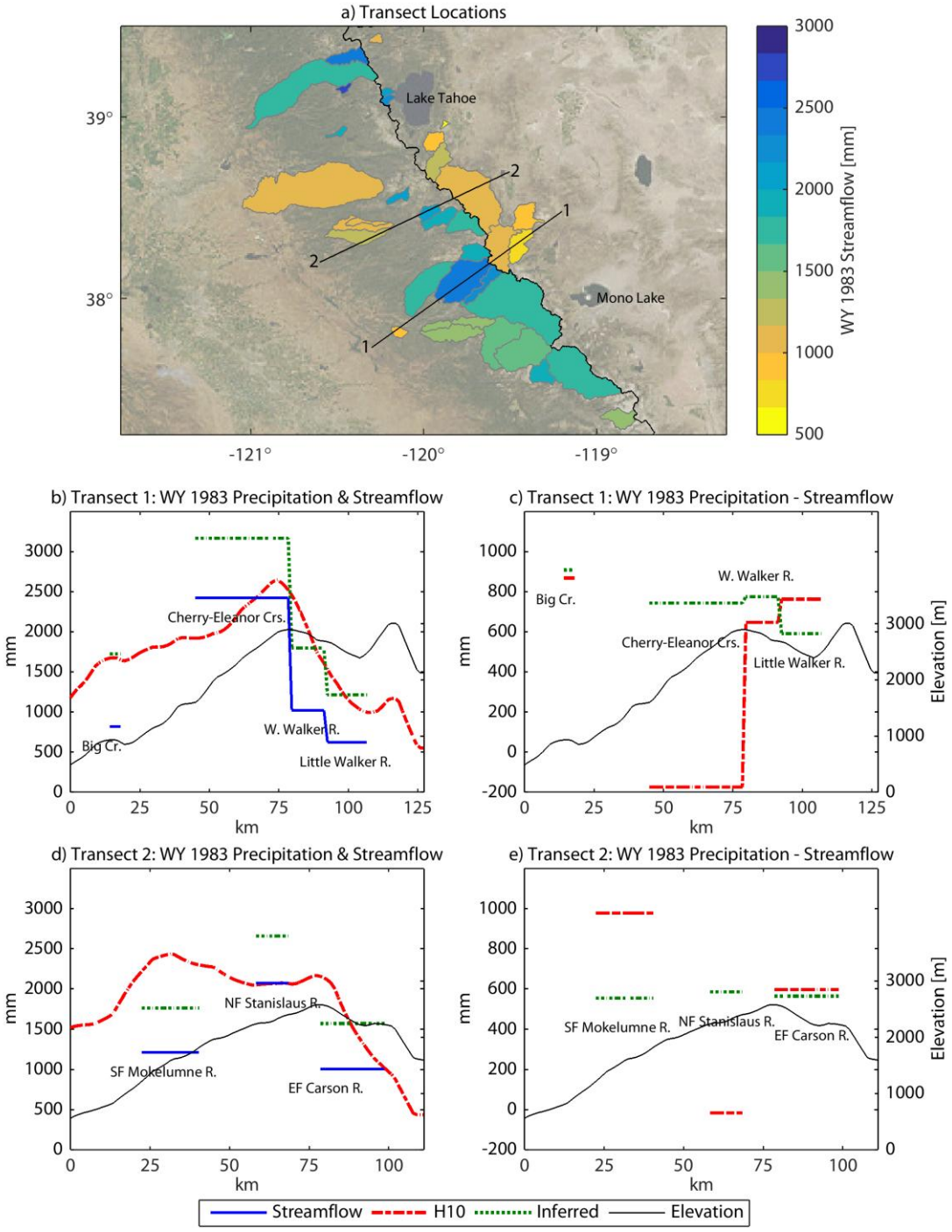


Figure 7. Cross-Sierra Nevada patterns of streamflow and precipitation. a) Inset of 1983 streamflow map, showing locations of two transects that pass from southwest to northeast across the range. b), d) Transects of water year 1983 streamflow and H10 and inferred precipitation, along with elevation. c), e) Precipitation (H10 and inferred) minus streamflow for the same transects. Streamflow, inferred precipitation, and precipitation minus streamflow are shown as the basin-mean for all points within the basin.

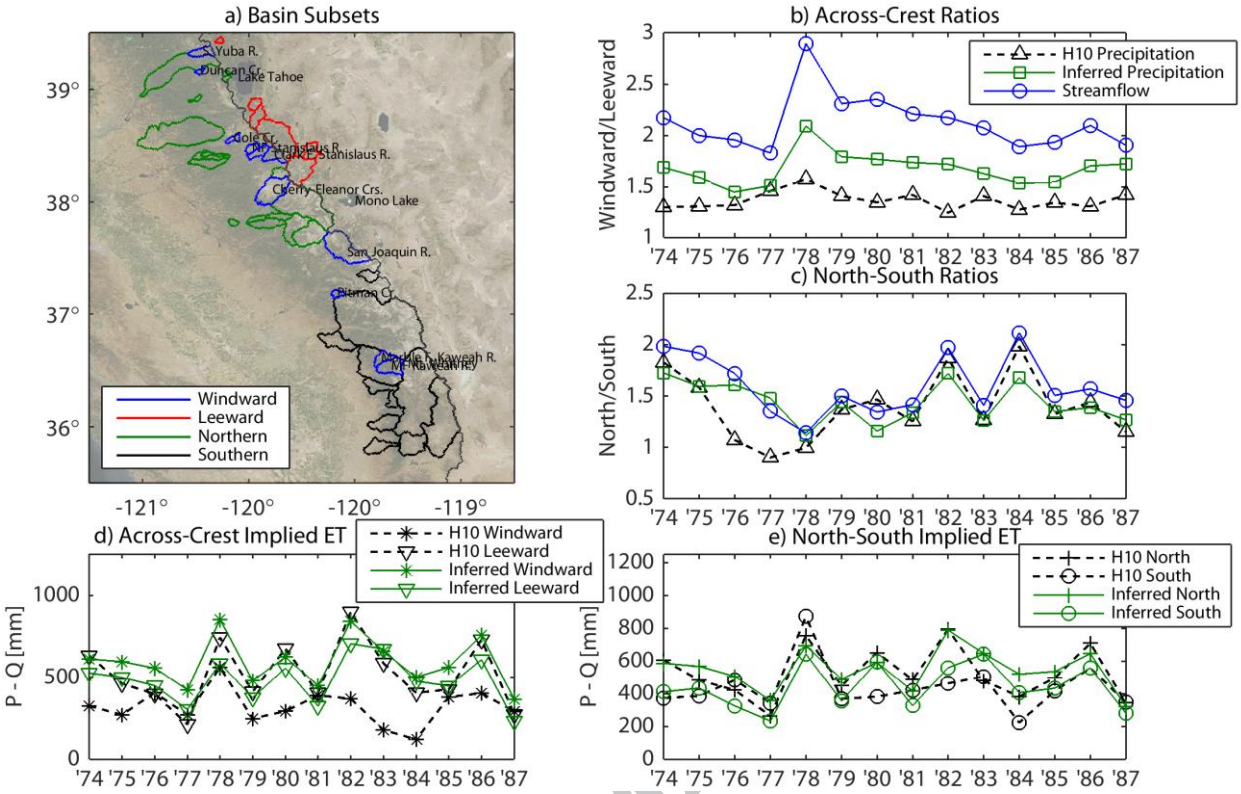


Figure 8. a) Map of basins indicating windward, leeward, northern and southern groups. Time series of windward-leeward (b) and north-south (c) ratios of precipitation and streamflow over water years 1974-1987. d) Time series of precipitation minus streamflow (implied ET) for the windward and leeward basins from H10 and inferred precipitation. e) Time series of implied ET for the northern and southern basins from H10 and inferred precipitation.

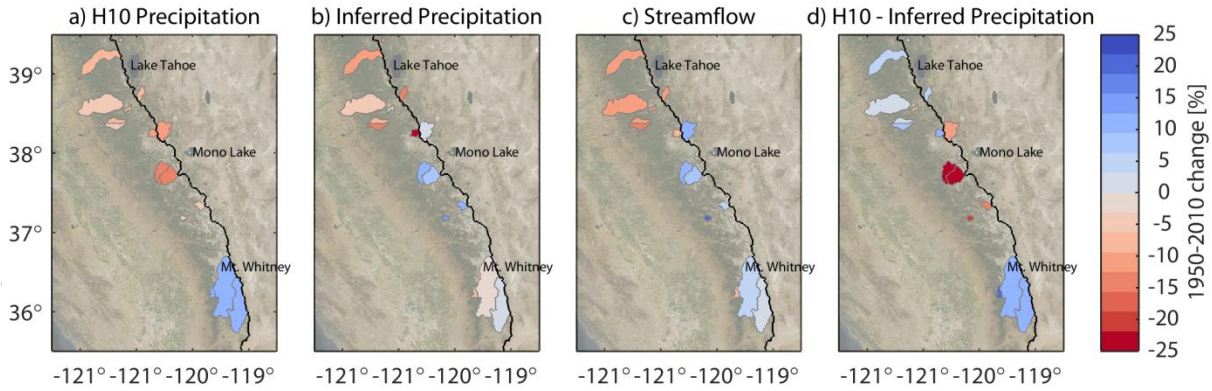


Figure 9. 1950-2010 trends in precipitation and streamflow over the Sierra Nevada, expressed as the 1950-2010 change in the best-fit line as a percentage of the 1950 best-fit value. a) Trends in basin-mean precipitation from the H10 dataset. b) Trends in inferred precipitation. c) Trends in streamflow. d) Differences between H10 and inferred precipitation trends.

ACCEPTED MANUSCRIPT

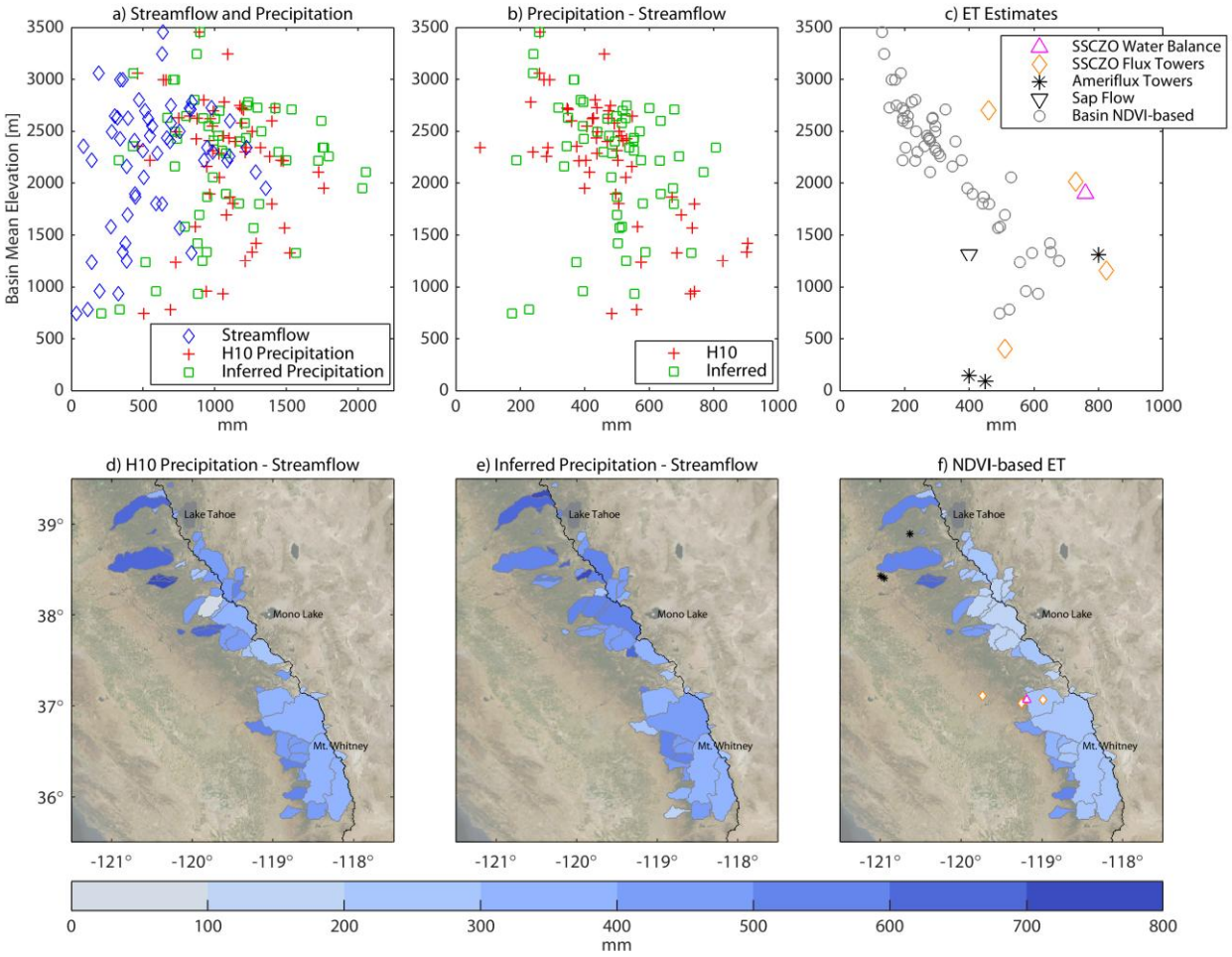


Figure 10. Patterns of precipitation, streamflow and ET over the Sierra Nevada domain. a) Long-term average streamflow and precipitation vs. mean elevation for each basin. b) Long-term average H10 and inferred precipitation minus streamflow (implied actual ET) for each basin. c) Elevational pattern of Sierra Nevada ET estimates: Southern Sierra Critical Zone Observatory flux towers (Goulden et al., 2012) and water balance (Bales et al., 2011) estimates of ET; Ameriflux tower ET estimates (Ichii et al., 2009; Kurpius et al., 2003); ET based on MODIS NDVI regression (Goulden et al., 2012) from water year 2003 NDVI for each basin. d) – f) Maps of basin-mean ET estimates from H10 precipitation, inferred precipitation, and MODIS NDVI regression, respectively. Flux tower locations are shown in f).

ACCEPTED

ACCEPTED MANUSCRIPT

References

Adam, J., Clark, E., Lettenmaier, D., 2006. Correction of global precipitation products for orographic effects. J. Clim. 19, 15–38. doi:http://dx.doi.org/10.1175/JCLI3604.1

Allen, R.G., Pereira, L.S., Raes, D., Smith, M., 1998. Crop evapotranspiration: Guidelines for computing crop water requirements - FAO Irrigation and drainage paper 56. Rome.

Anders, A.M., Roe, G.H., Durran, D.R., Minder, J.R., 2007. Small-Scale Spatial Gradients in Climatological Precipitation on the Olympic Peninsula. J. Hydrometeorol. 8, 1068–1081. doi:10.1175/JHM610.1

Anderson, E., 2006. Snow accumulation and ablation model–SNOW-17. On-line Doc.

Anderson, S.W., Rockwell, G.L., Friebel, M.F., Webster, M.D., 1996. Water Resources Data - California, Water Year 1996, Vol. 4 - U.S. Geological Survey Water-Data Report.

Baldassarre, G., Montanari, A., 2009. Uncertainty in river discharge observations: a quantitative analysis. Hydrol. Earth Syst. … 913–921.

Bales, R.C., Hopmans, J.W., O'Geen, A.T., Meadows, M., Hartsough, P.C., Kirchner, P., Hunsaker, C.T., Beaudette, D., 2011. Soil Moisture Response to Snowmelt and Rainfall in a Sierra Nevada Mixed-Conifer Forest. Vadose Zo. J. 10, 786. doi:10.2136/vzj2011.0001

Bristow, K., Campbell, G., 1984. On the relationship between incoming solar radiation and daily maximum and minimum temperature. Agric. For. Meteorol. 31, 159–166.

Caldwell, P., Chin, H.-N.S., Bader, D.C., Bala, G., 2009. Evaluation of a WRF dynamical downscaling simulation over California. Clim. Change 95, 499–521. doi:10.1007/s10584-009-9583-5

Christensen, L., Tague, C., Baron, J., 2008. Spatial patterns of simulated transpiration response to climate variability in a snow dominated mountain ecosystem. Hydrol. Process. 3588, 3576–3588. doi:10.1002/hyp

Clark, M., Slater, A.G., 2006. Probabilistic quantitative precipitation estimation in complex terrain. J. Hydrometeorol. 7, 3–22. doi:http://dx.doi.org/10.1175/JHM474.1

Clark, M.P., McMillan, H.K., Collins, D.B.G., Kavetski, D., Woods, R. a., 2011. Hydrological field data from a modeller's perspective: Part 2: process-based evaluation of model hypotheses. Hydrol. Process. 25, 523–543. doi:10.1002/hyp.7902

Clark, M.P., Slater, A.G., Rupp, D.E., Woods, R. a., Vrugt, J. a., Gupta, H. V., Wagener, T., Hay, L.E., 2008. Framework for Understanding Structural Errors (FUSE): A modular framework to diagnose differences between hydrological models. Water Resour. Res. 44, W00B02. doi:10.1029/2007WR006735

ACCEPTED MANUSCRIPT

Cosgrove, B.A., Lohmann, D., Mitchell, K.E., Houser, P.R., Wood, E.F., Schaake, J.C., Robock, A., Marshall, C., Sheffield, J., Duan, Q., Luo, L., Higgins, R.W., Pinker, R.T., Tarpley, J.D., Meng, J., 2003. Real-time and retrospective forcing in the North American Land Data Assimilation System (NLDAS) project. J. Geophys. Res. 108, 8842. doi:10.1029/2002JD003118

Cristea, N., Kampf, S., Burges, S., 2013. Revised coefficients for Priestley-Taylor and Makkink-Hansen equations for estimating daily reference evapotranspiration. J. Hydrol. Eng. 18, 1289–1300. doi:10.1061/(ASCE)HE.1943-5584.0000679.

Daly, C., Gibson, W., Taylor, G., 2002. A knowledge-based approach to the statistical mapping of climate. Clim. Res. 22, 99–113.

Daly, C., Halbleib, M., Smith, J.I., Gibson, W.P., Doggett, M.K., Taylor, G.H., Curtis, J., Pasteris, P.P., 2008. Physiographically sensitive mapping of climatological temperature and precipitation across the conterminous United States. Int. J. Climatol. 28, 2031–2064. doi:10.1002/joc.1688

Daly, C., Neilson, R., Phillips, D., 1994. A statistical-topographic model for mapping climatological precipitation over mountainous terrain. J. Appl. Meteorol. 33.

Dudhia, J., 1989. Numerical Study of Convection Observed during the Winter Monsoon Experiment Using a Mesoscale Two-Dimensional Model. J. Atmos. Sci. doi:10.1175/1520-0469(1989)046<3077:NSOCOD>2.0.CO;2

Flint, A.L., Flint, L.E., Dettinger, M.D., 2008. Modeling Soil Moisture Processes and Recharge under a Melting Snowpack. Vadose Zo. J. 7, 350. doi:10.2136/vzj2006.0135

Frei, C., Schar, C., 1998. A precipitation climatology of the Alps from high-resolution rain-gauge observations. Int. J. Climatol. 18.8, 873–900.

Goulden, M.L., Anderson, R.G., Bales, R.C., Kelly, a. E., Meadows, M., Winston, G.C., 2012. Evapotranspiration along an elevation gradient in California's Sierra Nevada. J. Geophys. Res. Biogeosciences 117, 1–13. doi:10.1029/2012JG002027

Goulden, M.L., Bales, R.C., 2014. Mountain runoff vulnerability to increased evapotranspiration with vegetation expansion. Proc. Natl. Acad. Sci. 111, 14071–14075. doi:10.1073/pnas.1319316111

Grubišić, V., Vellore, R.K., Huggins, A.W., 2005. Quantitative Precipitation Forecasting of Wintertime Storms in the Sierra Nevada: Sensitivity to the Microphysical Parameterization and Horizontal Resolution. Mon. Weather Rev. 133, 2834–2859. doi:10.1175/MWR3004.1

Gutmann, E.D., Rasmussen, R.M., Liu, C., Ikeda, K., Gochis, D.J., Clark, M.P., Dudhia, J., Thompson, G., 2012. A Comparison of Statistical and Dynamical Downscaling of Winter Precipitation over Complex Terrain. J. Clim. 25, 262–281. doi:10.1175/2011JCLI4109.1

ACCEPTED MANUSCRIPT

Hamlet, A., Lettenmaier, D., 2005. Production of Temporally Consistent Gridded Precipitation and Temperature Fields for the Continental United States. J. Hydrometeorol. 6, 330–336.

Hamlet, A.F., Carrasco, P., Deems, J.S., Elsner, M.M., Kamstra, T., Lee, C., Lee, S.-Y., Mauger, G., Salathe, E., Tohver, I., Whitely Binder, L., 2010. Final report for the Columbia Basin Climate Change Scenarios Project.

Hamlet, A.F., Mote, P.W., Clark, M.P., Lettenmaier, D.P., 2007. Twentieth-century trends in runoff, evapotranspiration, and soil moisture in the western United States. J. Clim. 20, 1468–1486. doi:10.1175/JCLI4051.1

Hamlet, A.F., Mote, P.W., Clark, M.P., Lettenmaier, D.P., 2005. Effects of temperature and precipitation variability on snowpack trends in the sestern United States. J. Clim. 18, 4545–4561. doi:10.1175/JCLI3538.1

Henn, B., Clark, M.P., Kavetski, D., Lundquist, J.D., 2015. Estimating mountain basin-mean precipitation from streamflow using Bayesian inference. Water Resour. Res. 51. doi:10.1002/2014WR016736

Henn, B., Clark, M.P., Kavetski, D., McGurk, B., Painter, T.H., Lundquist, J.D., 2016a. Combining Snow, Streamflow and Precipitation Gauge Observations to Infer Basin-Mean Precipitation. Water Resour. Res.

Henn, B., Newman, A.J., Livneh, B., Daly, C., Lundquist, J.D., 2016b. An assessment of differences in gridded precipitation datasets in complex terrain. J. Hydrol.

Holbrook, W.S., Riebe, C.S., Elwaseif, M., Hayes, J.L., Basler-Reeder, K., Harry, D.L., Malazian, A., Dosseto, A., Hartsough, P.C., Hopmans, J.W., 2014. Geophysical constraints on deep weathering and water storage potential in the Southern Sierra Critical Zone Observatory. Earth Surf. Process. Landforms 39, 366–380. doi:10.1002/esp.3502

Hong, S.-Y., Noh, Y., Dudhia, J., 2006. A New Vertical Diffusion Package with an Explicit Treatment of Entrainment Processes. Mon. Weather Rev. 134, 2318–2341. doi:10.1175/MWR3199.1

Hughes, M., Neiman, P.J., Sukovich, E., Ralph, M., 2012. Representation of the Sierra Barrier Jet in 11 years of a high-resolution dynamical reanalysis downscaling compared with long-term wind profiler observations. J. Geophys. Res. Atmos. 117, 1–18. doi:10.1029/2012JD017869

Ichii, K., Wang, W., Hashimoto, H., Yang, F., Votava, P., Michaelis, A.R., Nemani, R.R., 2009. Refinement of rooting depths using satellite-based evapotranspiration seasonality for ecosystem modeling in California. Agric. For. Meteorol. 149, 1907–1918. doi:10.1016/j.agrformet.2009.06.019

Kain, J.S., 2004. The Kain–Fritsch Convective Parameterization: An Update. J. Appl. Meteorol. 43, 170–181. doi:10.1175/1520-0450(2004)043<0170:TKCPAU>2.0.CO;2

ACCEPTED MANUSCRIPT

Kattelmann, R., Elder, K., 1991. Hydrologic characteristics and water-balance of an alpine basin in the Sierra-Nevada. Water Resour. Res. 27, 1553–1562. doi:10.1029/90WR02771

Kavetski, D., Franks, S.W., Kuczera, G., 2003. Confronting Input Uncertainty in Environmental Modelling, in: Duan, Q., Gupta, H. V., Sorooshian, S., Rousseau, A.N., Turcotte, R. (Eds.), Calibration of Watershed Models. Washington, D.C.: American Geophysical Union, pp. 49–68. doi:10.1029/WS006p0049

Kavetski, D., Kuczera, G., Franks, S.W., 2006a. Bayesian analysis of input uncertainty in hydrological modeling: 1. Theory. Water Resour. Res. 42, 1–9. doi:10.1029/2005WR004368

Kavetski, D., Kuczera, G., Franks, S.W., 2006b. Bayesian analysis of input uncertainty in hydrological modeling: 2. Application. Water Resour. Res. 42, W03408. doi:10.1029/2005WR004376

Kurpius, M.R., Panek, J. a., Nikolov, N.T., McKay, M., Goldstein, a. H., 2003. Partitioning of water flux in a Sierra Nevada ponderosa pine plantation. Agric. For. Meteorol. 117, 173–192. doi:10.1016/S0168-1923(03)00062-5

Le Moine, N., Hendrickx, F., Gailhard, J., Garcon, R., Gottardi, F., 2015. Hydrologically-aided interpolation (HAI) of daily precipitation and temperature fields in a meso-scale Alpine catchment. J. Hydrometeorol. doi:dx.doi.org/10.1175/JHM-D-14-0162.1

Lettenmaier, D.P., Alsdorf, D., Dozier, J., Huffman, G.J., Pan, M., Wood, E.F., 2015. Inroads of remote sensing into hydrologic science during the WRR era. Water Resour. Res. n/a–n/a. doi:10.1002/2015WR017616

Leydecker, A., Melack, J.M., 1999. Evaporation from snow in the central Sierra Nevada of California. Nord. Hydrol. 30, 81–108.

Livneh, B., Bohn, T.J., Pierce, D.W., Munoz-Arriola, F., Nijssen, B., Vose, R., Cayan, D.R., Brekke, L., 2015. A spatially comprehensive, hydrometeorological data set for Mexico, the U.S., and Southern Canada 1950–2013. Sci. Data 2, 150042. doi:10.1038/sdata.2015.42

Livneh, B., Deems, J.S., Schneider, D., Barsugli, J.J., Molotch, N.P., 2014. Filling in the gaps: Inferring spatially distributed precipitation from gauge observations over complex terrain. Water Resour. Res. 50, 8589–8610. doi:10.1002/2014WR015442

Lundquist, J., Cayan, D., Dettinger, M., 2003. Meteorology and hydrology in yosemite national park: A sensor network application. Inf. Process. Sens. … 518–528.

Lundquist, J.D., Hughes, M., Henn, B., Gutmann, E.D., Livneh, B., Dozier, J., Neiman, P., 2015. High-Elevation Precipitation Patterns: Using Snow Measurements to Assess Daily Gridded Datasets across the Sierra Nevada, California. J. Hydrometeorol. 16, 1773–1792. doi:10.1175/JHM-D-15-0019.1

ACCEPTED MANUSCRIPT

Lutz, J. a., van Wagtendonk, J.W., Franklin, J.F., 2010. Climatic water deficit, tree species ranges, and climate change in Yosemite National Park. J. Biogeogr. 37, 936–950. doi:10.1111/j.1365-2699.2009.02268.x

McMillan, H.K., Clark, M.P., Bowden, W.B., Duncan, M., Woods, R. a., 2011a. Hydrological field data from a modeller's perspective: Part 1. Diagnostic tests for model structure. Hydrol. Process. 25, 511–522. doi:10.1002/hyp.7841

McMillan, H.K., Jackson, B., Clark, M., Kavetski, D., Woods, R., 2011b. Rainfall uncertainty in hydrological modelling: An evaluation of multiplicative error models. J. Hydrol. 400, 83–94. doi:10.1016/j.jhydrol.2011.01.026

Minder, J.R., Durran, D.R., Roe, G.H., Anders, A.M., 2008. The climatology of small-scale orographic precipitation over the Olympic Mountains: Patterns and processes. Q. J. R. Meteorol. Soc. 134, 817–839. doi:10.1002/qj.258

Mitchell, K.E., Lohmann, D., Houser, P.R., Wood, E.F., Schaake, J.C., Robock, A., Cosgrove, B. a, Sheffield, J., Duan, Q., Luo, L., Higgins, R.W., Pinker, R.T., Tarpley, J.D., Lettenmaier, D.P., Marshall, C.H., Entin, J.K., Pan, M., Shi, W., Koren, V., Meng, J., Ramsay, B.H., Bailey, A. a, 2004. The multi-institution North American Land Data Assimilation System (NLDAS): Utilizing multiple GCIP products and partners in a continental distributed hydrological modeling system. J. Geophys. Res. 109, D07S90–. doi:10.1029/2003JD003823

Mlawer, E.J., Taubman, S.J., Brown, P.D., Iacono, M.J., Clough, S. a., 1997. Radiative transfer for inhomogeneous atmospheres: RRTM, a validated correlated-k model for the longwave. J. Geophys. Res. 102, 16663. doi:10.1029/97JD00237

Morrison, H., Thompson, G., Tatarskii, V., 2009. Impact of Cloud Microphysics on the Development of Trailing Stratiform Precipitation in a Simulated Squall Line: Comparison of One- and Two-Moment Schemes. Mon. Weather Rev. 137, 991–1007. doi:10.1175/2008MWR2556.1

Mote, P.W., Hamlet, A.F., Clark, M.P., Lettenmaier, D.P., 2005. Declining Mountain Snowpack in Western North America. Bull. Am. Meteorol. Soc. 86, 39–49. doi:10.1175/BAMS-86-1-39

Newman, A.J., Clark, M.P., Craig, J., Nijssen, B., Wood, A., Gutmann, E., Mizukami, N., Brekke, L., Arnold, J.R., 2015. Gridded Ensemble Precipitation and Temperature Estimates for the Contiguous United States. J. Hydrometeorol. 16, 2481–2500. doi:10.1175/JHM-D-15-0026.1

NRCS, 2007. Soil Survey of Yosemite National Park, California.

PRISM Climate Group, 2015. Descriptions of PRISM Spatial Climate Datasets for the Conterminous United States.

ACCEPTED MANUSCRIPT

Raleigh, M.S., Lundquist, J.D., Clark, M.P., 2015. Exploring the impact of forcing error characteristics on physically based snow simulations within a global sensitivity analysis framework. Hydrol. Earth Syst. Sci. 19, 3153–3179. doi:10.5194/hess-19-3153-2015

Rasmussen, R., Baker, B., Kochendorfer, J., Meyers, T., Landolt, S., Fischer, A.P., Black, J., Theriault, J., Kucera, P., Gochis, D., Smith, C., Nitu, R., Hall, M., Cristanelli, S., Gutmann, E., 2011a. The NOAA/FAA/NCAR Winter Precipitation Test Bed: How Well Are We Measuring Snow? Bull. Am. Meteorol. Soc. 811–829. doi:10.1175/BAMS-D-11-00052.1

Rasmussen, R., Liu, C., Ikeda, K., Gochis, D., Yates, D., Chen, F., Tewari, M., Barlage, M., Dudhia, J., Yu, W., Miller, K., Arsenault, K., Grubišić, V., Thompson, G., Gutmann, E., 2011b. High-Resolution Coupled Climate Runoff Simulations of Seasonal Snowfall over Colorado: A Process Study of Current and Warmer Climate. J. Clim. 24, 3015–3048. doi:10.1175/2010JCLI3985.1

Renard, B., Kavetski, D., Kuczera, G., Thyer, M., Franks, S.W., 2010. Understanding predictive uncertainty in hydrologic modeling: The challenge of identifying input and structural errors. Water Resour. Res. 46, W05521. doi:10.1029/2009WR008328

Rockwell, G.L., Anderson, S.W., Hayes, P.D., 1996a. Water Resources Data - California, Water Year 1996, U.S. Geological Survey Water-Data Report.

Rockwell, G.L., Hayes, P.D., Agajanian, J., 1996b. Water Resources Data - California, Water Year 1996, Vol. 1 - U.S. Geological Survey Water-Data Report.

Roe, G.H., 2005. Orographic Precipitation. Annu. Rev. Earth Planet. Sci. 33, 645–671. doi:10.1146/annurev.earth.33.092203.122541

Rose, K., Graham, R., Parker, D., 2003. Water source utilization by Pinus jeffreyi and Arctostaphylos patula on thin soils over bedrock. Oecologia 134, 46–54. doi:10.1007/s00442-002-1084-4

Sieck, L.C., Burges, S.J., Steiner, M., 2007. Challenges in obtaining reliable measurements of point rainfall. Water Resour. Res. 43. doi:10.1029/2005WR004519

Skamarock, W.C., Klemp, J.B., 2008. A time-split nonhydrostatic atmospheric model for weather research and forecasting applications. J. Comput. Phys. 227, 3465–3485. doi:10.1016/j.jcp.2007.01.037

Skamarock, W.C., Klemp, J.B., Dudhi, J., Gill, D.O., Barker, D.M., Duda, M.G., Huang, X.-Y., Wang, W., Powers, J.G., 2008. A Description of the Advanced Research WRF Version 3. Tech. Rep. 113. doi:10.5065/D6DZ069T

Slack, J.R., Landwehr, J.M., 1992. Hydro-Climatic Data Network (HCDN): A U. S. Geological Survey streamflow data set for the United States for the study of climate variations, 1874-1988. U.S. Geol. Surv. Open-File Rep. 92-129.

ACCEPTED MANUSCRIPT

Stephenson, N.L., 1998. Actual evapotranspiration and deficit: biologically meaningful correlates of vegetation distribution across spatial scales. J. Biogeogr. 25, 855–870. doi:10.1046/j.1365-2699.1998.00233.x

Tewari, M., Chen, F., Wang, W., Dudhia, J., LeMone, M.A., Mitchell, K., Ek, M., Gayno, G., Wegiel, J., Cuenca, R.H., 2004. Implementation and verification of the unified noah land surface model in the WRF model, in: Bulletin of the American Meteorological Society. pp. 2165–2170.

Thornton, P.E., Running, S.W., White, M.A., 1997. Generating surfaces of daily meteorological variables over large regions of complex terrain. J. Hydrol. 190, 214–251. doi:10.1016/S0022-1694(96)03128-9

Thyer, M., Renard, B., Kavetski, D., Kuczera, G., Franks, S.W., Srikanthan, S., 2009. Critical evaluation of parameter consistency and predictive uncertainty in hydrological modeling: A case study using Bayesian total error analysis. Water Resour. Res. 45, W00B14. doi:10.1029/2008WR006825

Viviroli, D., Dürr, H.H., Messerli, B., Meybeck, M., Weingartner, R., 2007. Mountains of the world, water towers for humanity: Typology, mapping, and global significance. Water Resour. Res. 43, 1–13. doi:10.1029/2006WR005653

Wayand, N.E., Hamlet, A.F., Hughes, M., Feld, S.I., Lundquist, J.D., 2013. Intercomparison of Meteorological Forcing Data from Empirical and Mesoscale Model Sources in the North Fork American River Basin in Northern Sierra Nevada, California. J. Hydrometeorol. 14, 677–699. doi:10.1175/JHM-D-12-0102.1

Westrick, K., Mass, C., Colle, B., 1999. The limitations of the WSR-88D radar network for quantitative precipitation measurement over the coastal western United States. Bull. Am. … 2289–2298.

Xia, Y., Mitchell, K., Ek, M., Cosgrove, B., Sheffield, J., Luo, L., Alonge, C., Wei, H., Meng, J., Livneh, B., Duan, Q., Lohmann, D., 2012. Continental-scale water and energy flux analysis and validation for North American Land Data Assimilation System project phase 2 (NLDAS-2): 2. Validation of model-simulated streamflow. J. Geophys. Res. 117, D03110. doi:10.1029/2011JD016051

ACCEPTED MANUSCRIPT

Highlights – Sierra Inferred Precipitation – Henn et al. 2016

- We use unimpaired observations from 56 long-term stream gauges in the Sierra Nevada
- We infer precipitation from streamflow for each basin-year with lumped hydrologic models
- For each year precipitation inferred from streamflow compared to gridded estimates
- Gridded estimates underestimate precipitation in basins favored for upslope flow
- Precipitation inferred from streamflow reveals inter-annual spatial variability

ACCEPTED MANUSCRIPT